Structures 44 (2022) 988–1010

Contents lists available at ScienceDirect

Structures

journal homepage: www.elsevier.com/locate/structures

Behaviour and design of the 'lockbolt' demountable shear connector for sustainable steel-concrete composite structures

Jun He [a,b], Ahmed S.H. Suwaed [c], George Vasdravellis [d,*], Sihao Wang [e]

[a] School of Civil Engineering, Changsha University of Science and Technology, China
[b] Institute for Infrastructure and Environment, Heriot-Watt University, UK
[c] Department of Reconstruction and Projects, University of Baghdad, Iraq
[d] Institute for Infrastructure and Environment, Heriot-Watt University, UK
[e] Department of Bridge Engineering, Tongji University, China

ARTICLE INFO

Keywords:
Demountable shear connector
Lockbolt
Grout-filled tube
Pushout test
Finite element model
Shear strength
Relative slip

ABSTRACT

In order to promote sustainable steel-concrete composite structures, special shear connectors that can facilitate deconstruction are needed. A lockbolt demountable shear connector (LB-DSC), including a grout-filled steel tube embedded in the concrete slab and fastened to a geometrically compatible partial-thread bolt, which is bolted on the steel section's top flange of a composite beam, was proposed. The main drawback of previous similar demountable bolts is the sudden slip of the bolt inside its hole. This bolt has a locked conical seat lug that is secured inside a predrilled compatible counter-sunk hole in the steel section's flange to provide a non-slip bolt-flange connection. Deconstruction is achieved by demounting the tube from the top of the slab by unfastening using a simple modified wrench. The mechanical behaviour of the proposed connector is assessed by four pushout tests that were conducted per Eurocode 4 recommendations. The tests showed high shear resistance, and high stiffness as compared to other DSCs, while the slip capacity results classified the LB-DSC as a ductile shear connector according to Eurocode 4. A refined nonlinear finite element model (FEM) was validated through the tests and reliably reproduced the experimental behaviour. Consequently, the calibrated FEM model was applied to carry out extensive parametric analyses to investigate the strength and geometry effects of concrete slab, infilled grout, tube, and bolt on the structural behaviour of the LB-DSC. On the basis of numerical and experimental results, a design equation is derived to predict the shear resistance of the LB-DSC.

1. Introduction

In order to achieve future sustainability targets, such as the "Net zero carbon target" [1] and the Green Deal [2,3], more attention should be paid to the construction sector, because the production of most commonly used construction materials (e.g. the cement and steel) lead to 15 % of the world human-induced CO_2 emissions. Furthermore, it is anticipated that the material demand will be doubled in the next 20 years, indicating that a more responsible use of natural resources is highly needed [4]. Furthermore, considerable quantities of waste sent to landfill due to construction and demolition activities. In order to maintain a sustainable international environment, using demountable and reusable structural systems can be the solution [5].

Steel-concrete structures are extensively used in buildings and bridges, thanks to the composite action of the individual benefits of steel and concrete, high strength and stiffness, and accelerated prefabricated construction [6–10]. The shear connection type between steel and concrete components is inherently significant, because it enables the composite section to behave as one unit. In addition, the connection must be able to effectively resist separation between the two components [11–15]. Among various shear connectors in steel–concrete composite structure, headed studs have become the most practical type for achieving the composite action due to their standardized welding technique, good mechanical performance, and extensive research data available [16–21].

However, from the viewpoint of sustainable development, composite beams with welded headed studs are not recommended because of the difficulty of detaching the concrete slab from the supporting steel sections at the end-of-life of a structure, or because of the excessive downtime required to repair or replace a deteriorated composite bridge

* Corresponding author at: Heriot-Watt University, Riccarton, EH14 4AS, UK.
E-mail address: g.vasdravellis@hw.ac.uk (G. Vasdravellis).

https://doi.org/10.1016/j.istruc.2022.08.062
Received 23 March 2022; Received in revised form 21 June 2022; Accepted 12 August 2022
Available online 22 August 2022

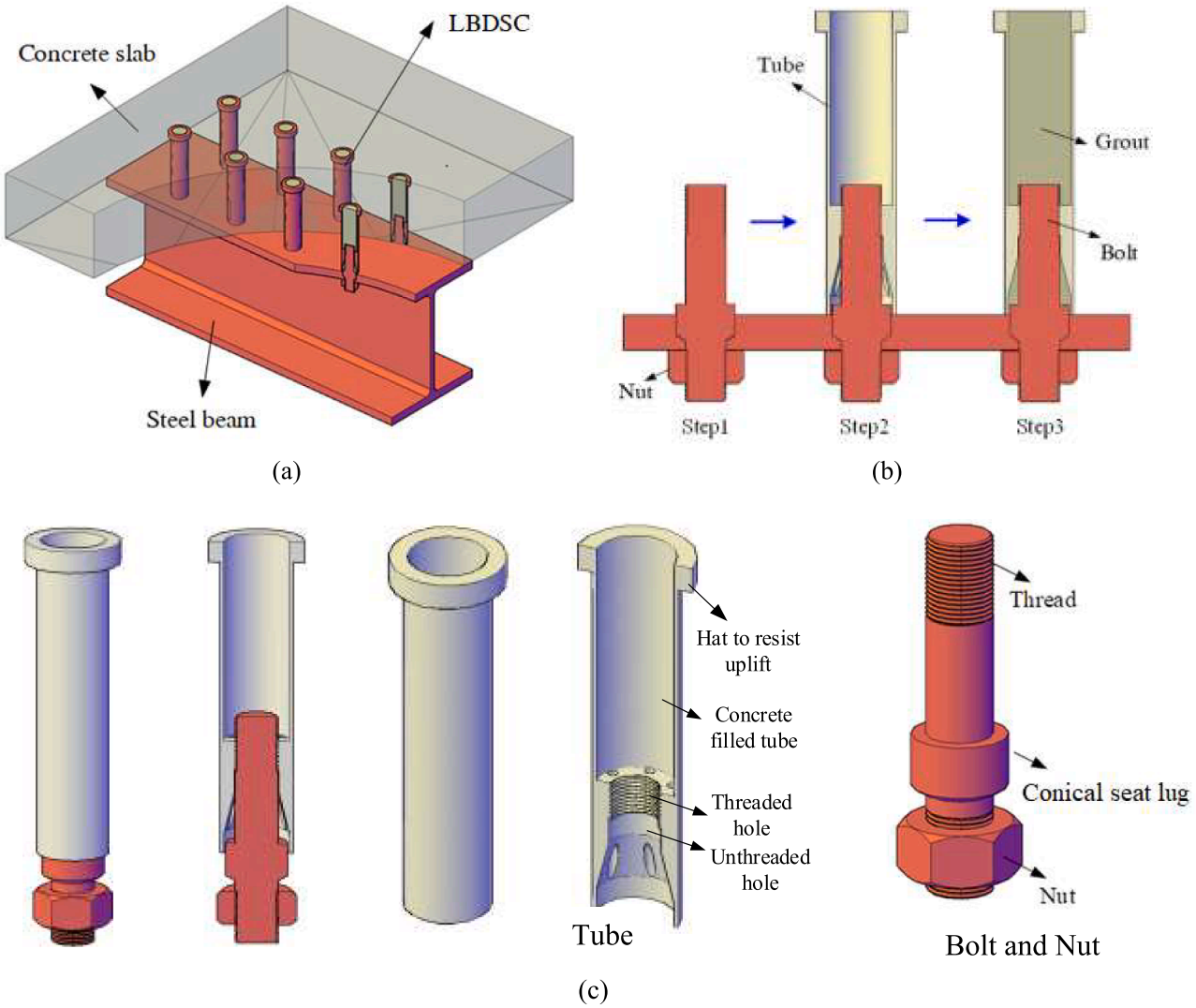

Fig. 1. (a) Composite girder with LB-DSCs; (b) Assembly of LB-DSC; (c) Details of LB-DSC.

deck. Thus, recently some research has been conducted to develop novel shear connectors that allow for an easier separation of concrete slabs from the steel sections and reuse of structural components.

Pre-tensioned high strength friction-grip (HSFG) bolts were experimentally investigated as shear connectors [22–24]. Three types of post-installed shear connectors to retrofit non-composite bridges [25,26] were tested and showed significant increase in resistance and stiffness as well as good fatigue performance. Bolt shear connectors were inspected and showed low stiffness in comparison with headed studs [27,28]. The behaviour of HSFG bolts in composite beams with geopolymer precast concrete slabs was examined and identified significant shear resistance, large slip capacity [29], and enough absorbed energy capacity when subjected to low-cycle high-amplitude loading [30,31]. A novel connector consisted of a short bolt, long bolt, and coupler was proposed, however, a ductile behaviour can only be obtained when the diameter of the bolts was no less than 27 mm [32]. In addition, extensive research has been conducted [33–36] on shear bolts machined from headed studs. The results showed comparable resistance, higher slip capacity, but about half the initial stiffness of the headed studs due to unavoidable clearance between the bolt collar and its hole. Moreover, blind bolts were proposed [37] to retrofit composite beams and found that they had higher shear resistance in comparison to headed studs, but with smaller stiffness. The blind bolts were also tested in full-scale composite beams [38], under sustained loads [39], and under dynamic loading [40,41], and showed comparable behaviour to beams with headed studs. Recently, highly ductile demountable steel hollow sections as shear connectors for hollow-core precast slabs were developed [42,43] and showed higher stiffness and slip capacity compared to welded studs.

Previous tests on bolts shear connector revealed an unfavourable sudden slip under serviceability limit state (SLS) due to bolts sliding inside their holes when friction resistance is exceeded, which may prevent their possible application in practice. Thus, epoxy resin injected inside the bolt holes was used [44]; however, the slip capacity was still rather limited. Preloaded bolts based on steel–concrete friction resistance were tested by pushout and beam tests and showed full-interaction performance under SLS [45,46]. A locked-nut DSC was proposed, using a cone-shaped nut that "locks" into counter-shaped corresponding holes in the steel section flange to avoid the sudden slip [47]. Presently, a welded demountable connector to eliminate the sudden slip was validated experimentally and numerically [48,49]. Inspired by the concept described in [47], the authors proposed a lockbolt demountable shear connector (LB-DSC) to eliminate the sudden slip as well the tolerance issues in the holes drilled in the flange, and to allow for an easy separation of the slabs from the top of the composite floor.

1.1. LBDSC description

Fig. 1a shows the details of the proposed LB-DSC. It includes a grout-

(a) (b) (c)

Fig. 2. Specimen preparation in the Lab: (a) Assembled shear connector without grout on steel section; (b) filled in grout, installed reinforcement cage and formwork; (c) cast concrete.

filled headed steel tube with internal partial thread fastened over a compatible partial thread bolt (Fig. 1c). The bolt has a conical lug that fits in compatible pre-drilled counter-sunk conical seat holes in the steel flanges and, therefore, excludes the sudden slip and resolves any tolerance issues. The headed steel tube with 33–37 mm external diameter (depending on the bolt diameter and thickness of tube) is a machined monolithic unit. The bottom thicker segment of the tube includes three parts from up to down: A threaded part to connect the tube to the bolt; then an enlarged unthreaded hole to hide bolt threads, preventing shear fracture through bolt's thread; next, a transition chamfered hole, to decrease stress concentration. To improve the shear resistance and stiffness of the LB-DSC, flowable grout should be filled into the tube and reached the bottom of the bolt though six longitudinal holes passed through the previous three parts, as shown in Fig. 1(c).

The construction procedure of the LB-DSC is depicted in Fig. 1b. Step 1: counter-sunk holes were bored on the steel section's flange, the partial-thread bolts with conical seat lug were placed inside the holes and fastened through the nut below the flange; Step 2: firmly hand-tightening the tube to the bolt; Step 3: The tube was filled with flowable grout; Step 4: Steel reinforcements were arranged and concrete was poured for the slab.

The deconstruction can be realized by loosening the nut shown in (b) and (c) of Fig. 1 from the bottom face of the steel–concrete composite beam, or, preferably, by loosening the tube from the top face using an electric or mechanical compatible wrench. Thus, the concrete slab and steel section can be easily detached from each other; and both can be reused in other sites.

The structural behaviour of the LB-DSC was checked using a series of pushout tests using a bespoke horizontal testing arrangement to imitate real beam conditions in [50]. The results indicated that the LBDSC has high shear resistance, stiffness, and slip capacity; however, the presence of non-negligible uplift forces as a result of the specific horizontal test setup, implied that further investigation is needed to understand the shear performance of the LBDSC and to propose accurate design equations.

Therefore, this paper presents a series of pushout tests that were carried out following the standard testing procedure of Eurocode 4 [51] to investigate the structural behaviour of the LB-DSC. A detailed finite element method (FEM) model considering material and contact nonlinearity was created and calibrated against the experimental results. Then, the calibrated FEM model was applied to perform parametric analyses to study the effects of concrete strength of the slab, bolt diameter/strength, steel tube thickness/strength, and presence/strength of infill grout on the shear resistance and stiffness of the LB-DSC. Finally, design equations for the prediction of the shear resistance of the LB-DSC are proposed to facilitate the application of the proposed connector in sustainable steel–concrete composite buildings.

2. Experimental programme

2.1. Test specimens

To investigate the shear performance of the LB-DSC, four standard pushout test specimens in accordance with Eurocode 4 [51] were fabricated, as shown in Fig. 2. The test specimen comprised of 600-mm long HEB260 steel section attached to two concrete slabs (650 × 600 × 150 mm), using two or four LB-DSCs in each slab. Holes with counter-sunk conical seat were drilled in each steel section, then partial thread bolts, as described in section 1.1, with compatible conical lug were locked inside these holes creating a stop mechanism against sudden slip below SLS. Headed tubes with compatible partial internal thread were fasten over each bolt. Flowable grout of QuickCEM with characteristics of quick setting and hardening were poured inside each tube to accelerate test specimens' fabrication process. Two layers of Ø10 mm deformed rebars were placed in each slab. The details of the pushout test specimens are shown in Fig. 3. Specimens LB-DSC (1, 3 and 4) used the flowable grout, while LB-DSC2 did not. In addition, the effects of the compressive strength of concrete slab (50.4 or 63.3 MPa), number of connectors (2 or 4) in each slab and loading procedure: Monotonic (M) and Cyclic (C) loading were considered, as shown in Table 1.

2.2. Material properties

The mechanic properties of grout mix and in-situ concrete of test specimens were obtained by concrete compression tests. Three concrete/grout cubes (100 mm as per BSI [52]) were prepared on the same date as the corresponding specimen using the same fresh concrete and tested together with the corresponding pushout test. Table 1 summarizes the average strengths.

The material properties of the tube and bolt were acquired from standard tensile coupon tests [53] including the modulus of elasticity, the yield stress (0.2 % proof stress), the tensile strength and corresponding tensile strain. Table 2 lists the results as average values of three identical coupons. Moreover, the engineering stress–strain curves for tube and bolt are shown in Fig. 7.

2.3. Test setup

A hydraulic actuator with force capacity of 2000 kN and displacement capacity of 120 mm was applied to move the steel section in relative to the attached concrete slabs using a stiff steel plate, as indicated in Fig. 4. A layer of plaster gypsum of high strength was used to embed the bottom of concrete slabs on the rigid plate. Belts, shown in Fig. 4, were barely attached around the specimens to prevent the slabs from falling sideway once the connectors are disconnected.

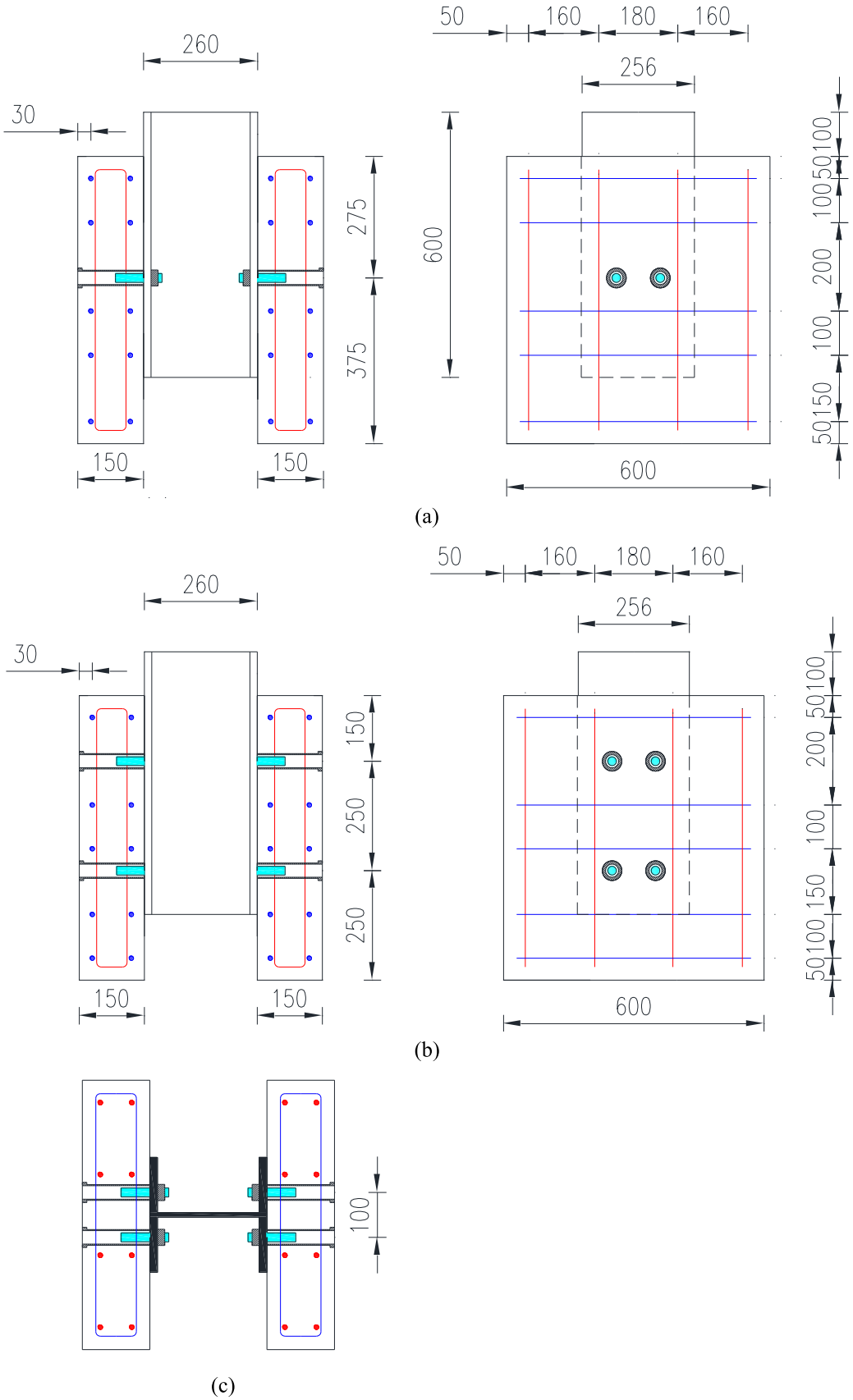

Fig. 3. Details of test specimens (unit: mm): elevation and side view of (a) LB-DSC1 to 3 and (b) LB-DSC4; (c) plan view of all LB-DSCs; (d) steel tube; (e) partly threaded conical bolt (f) counter-sunk hole in steel beam flange.

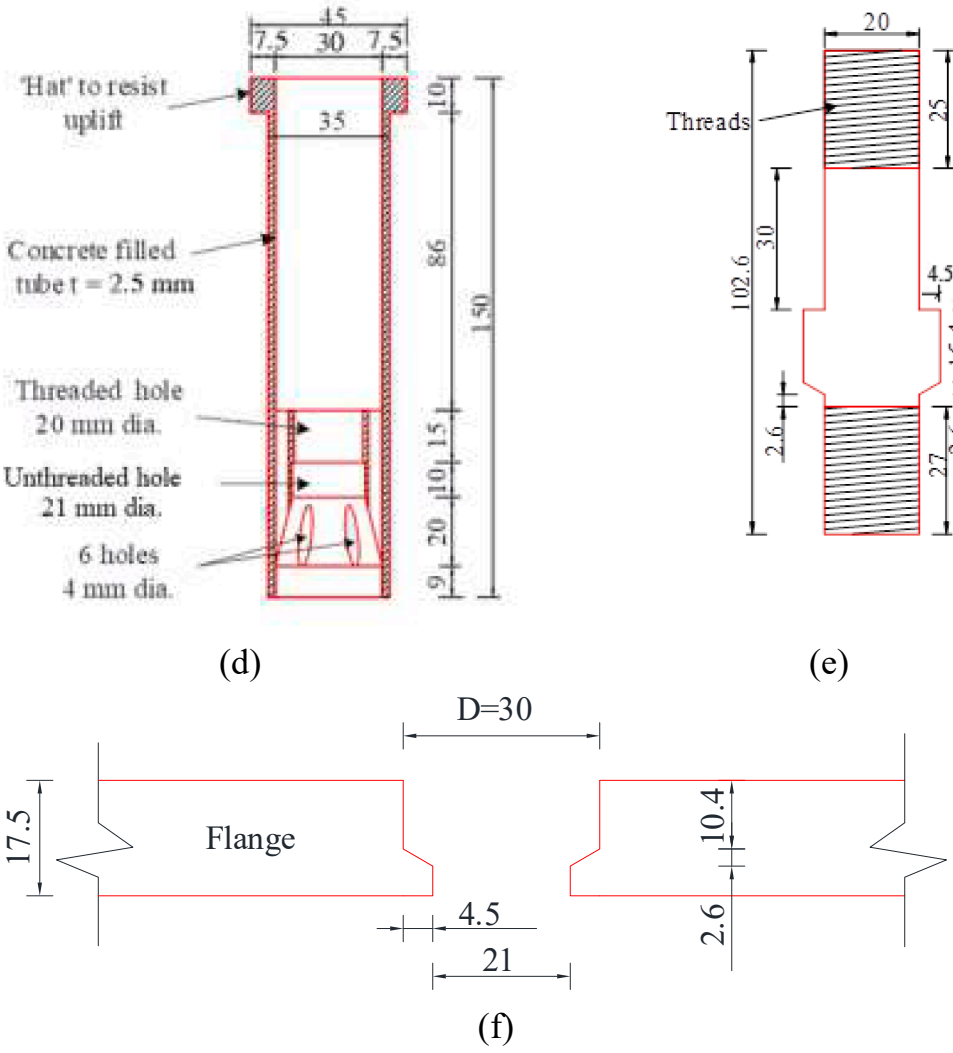

Fig. 3. (*continued*).

Table 1
Push out test specimens.

Specimen name	Concrete slab strength (N/mm^2)	Grout strength (N/mm^2)	Bolt diameter (mm)	Tube thickness (mm)	Number of connectors	Loading procedure
LB-DSC1	50.4	48	20	2.5	2	M
LB-DSC2	50.4	No grout	20	2.5	2	C + M
LB-DSC3	63.3	48	20	2.5	2	C + M
LB-DSC4	50.4	48	20	2.5	4	C + M

Table 2
Material properties of steel.

Coupon	Modulus of elasticity (GPa)	Yield stress (MPa)	Tensile stress (MPa)	Strain at ultimate stress
Bolt	210	818	990	0.090
Tube	205	333	645	0.188

2.4. Loading procedure and instrumentation

Fig. 5 shows the loading procedure that was adopted from Eurocode 4 and includes 25 load cycles between 5 and 40 % of the estimated ultimate load, followed by an imposed quasi-static monotonic load until failure of the specimen or until load drop by 20 % with respect to the peak load. The load was applied using a 0.005 mm/s displacement control. The recorded shear resistance by the loadcell is the division of ultimate load over the number of LB-DSC.

Fig. 4 shows the instrumentation used for the specimens. Two or four Linear Variable Differential Transformers (LVDTs), vertically mounted at the level of each connector, were used to measure the relative slip between the steel section and the concrete slab, while the separation at the steel–concrete interface was obtained using two LVDTs horizontally mounted near the connectors. All the devices were connected to a data logger and the data were recorded at 10 Hz rate of continues data-recording.

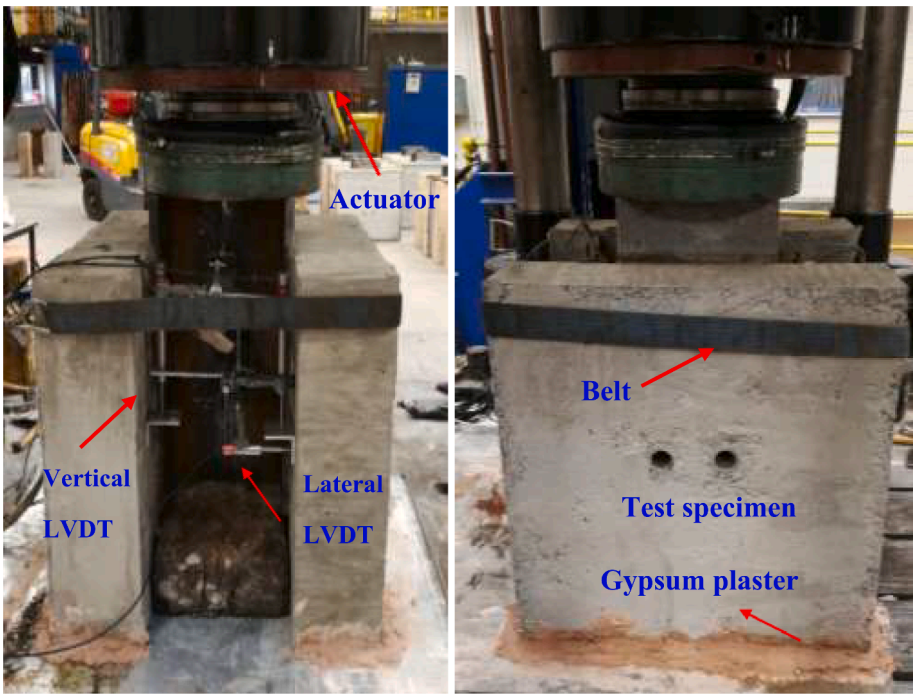

Fig. 4. Test setup.

3. Finite element model

3.1. Model description

Abaqus, the nonlinear FEM program [54], was used to simulate a quarter of pushout test specimen as shown in Fig. 6. The 3-dimensional 8-node reduced integration solid element (C3D8R) was used to model the steel section, concrete slab, infilled grout, bolts, nuts, and steel tube. The rebar mesh was simulated using (T3D2) 2-node truss element. The overall mesh used to model tube and bolt was 2 mm to give more precise predictions of the load-slip curves and failure modes.

Formulations of hard contact and penalty friction were employed to simulate the following interfaces: concrete slab-tube, grout-bolt, grout-tube, and bolt lug-countersunk hole. The friction coefficients were set as 0.4 for steel–concrete interfaces and 0.25 for steel-steel interfaces, respectively, which were determined through parametric sensitivity analysis and verified by the comparison of load-slip curves from FE analysis with those from previous test results [49,50,55]. The thread-to-thread connections in the bolt – tube bolting, as well in the bolt – nut bolting, were simulated using tie constraints. Complete bond (i.e. without considering slip or debonding) was assumed between reinforcements and the adjacent concrete.

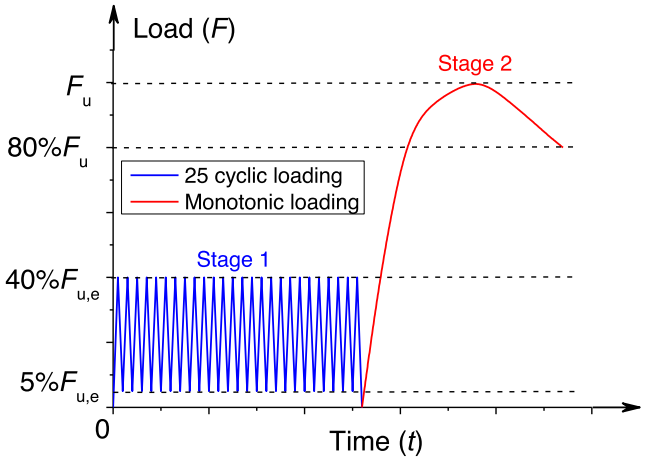

Fig. 5. Loading procedure.

The bottom of the rigid plate was assumed to be fully fixed, as shown in Fig. 6a. Planes 'A' and 'B' of steel section and concrete slab represent the symmetry boundary conditions. A displacement rate of 0.005 mm/s was enforced on the steel section upper part to simulate the experimental program.

3.2. Material modelling

3.2.1. Model of steel

A bi-linear elastic–plastic stress–strain curve was used to represent the stress–strain curve of the steel section (S355) and the steel reinforcements (S500), using nominal material characteristics. The true stress–strain curve of the high strength bolt and the steel tube were chosen based on the standard tensile tests, as displayed in Fig. 7a and b, respectively.

3.2.2. Model of concrete and grout

Fig. 8 shows uniaxial compressive and tensile stress–strain curve that represent the nonlinear behaviour of concrete and grout. Three parts represent the relation of stress (σ_c) and strain (ε_c) for concrete in compression. The first part (Eqs. (1) and (2)) is when the stress is below 0.4 f_c, according to *fib*-2010 [56], where f_c is the cylinder concrete compressive strength. The strain corresponding to the peak stress f_c is defined as peak strain ε_{cp}, and the value is equivalent to 0.0025.

$$\sigma_{c1} = E_c \varepsilon_c \tag{1}$$

$$E_c = E_{c0} \cdot \alpha_E \cdot (f_c/10)^{1/3} \tag{2}$$

where E_c is the modulus of elasticity of concrete (GPa); $E_{c0} = 21.5$ GPa; $\alpha_E = 1.0$ for quartzite aggregates.

The second part is the nonlinear parabolic portion (Eq. (3)) ranging from 0.4 f_c to f_c, as follows:

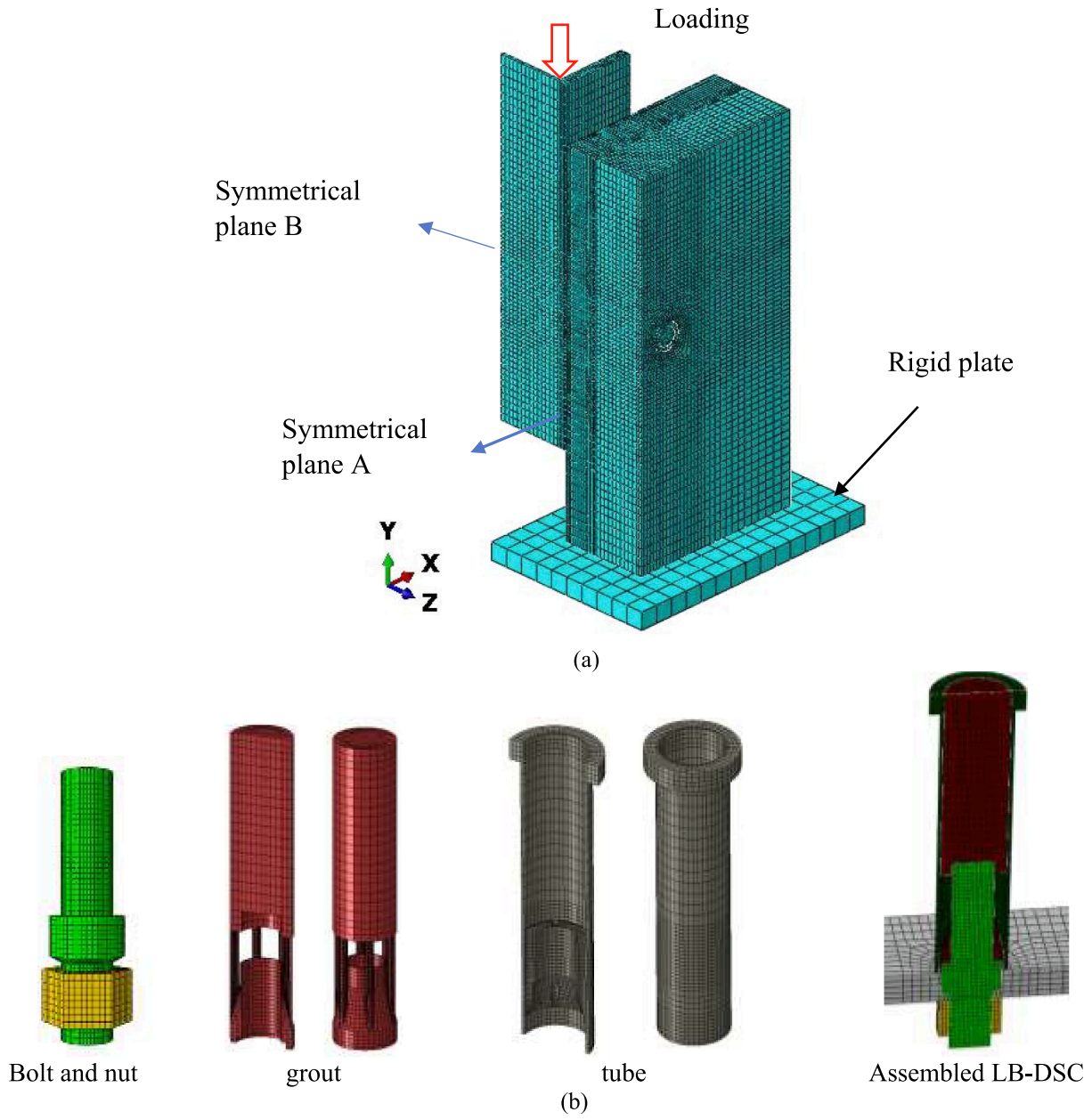

Fig. 6. Finite element model of pushout test: (a) Model of the specimen; (b) Mesh details of the LB-DSC.

$$\sigma_{c2} = f_c \frac{E_c\varepsilon_c/f_c - (\varepsilon_c/\varepsilon_{cp})^2}{1 + (E_c\varepsilon_c/f_c - 2\varepsilon_c/\varepsilon_{cp})} \tag{3}$$

The third part of the stress–strain curve is a descending linear branch (Eq. (4)). The stress at the ultimate strain ε_{cu} is assumed to be 0.85 f_c.

$$\sigma_{c3} = f_c\left(1 - 0.15\frac{\varepsilon_c - \varepsilon_{cp}}{\varepsilon_{cu}/\varepsilon_{cp}}\right) \tag{4}$$

A linear stress–strain relationship was implemented for the uncracked concrete section under tension. The modulus of elasticity in tension was presumed the same as that in compression. After the concrete section cracks, a nonlinear relationship of stress-crack width (Eq. (5)), is assumed.

$$\frac{\sigma_t}{f_t} = \left[1 + \left(c_1\frac{w}{w_c}\right)^3\right]e^{-c_2\frac{w}{w_c}} - \frac{w}{w_c}\left(1 + c_1^3\right)e^{-c_2} \tag{5}$$

where σ_t and f_t are the tensile stress and ultimate strength of concrete, respectively (MPa); w is the crack width (mm); w_c is the crack width when the stress is completely released, $w_c = 5.14G_F/f_t$ (mm); G_F is the fracture energy needed for the creation of a unit area of stress-free crack, (N/mm); c_1 and c_2 are the constants: $c_1 = 3$ and $c_2 = 6.93$.

Abaqus model of concrete damage plasticity (CDP) was adopted to describe the degraded response of concrete, which assumes that tensile cracking and compressive crushing are two main failures, their degraded degrees are expressed as d_c (Eq. (6)) and d_t (Eq. (7)), respectively.

$$d_c = 1 - \frac{\sigma_c}{E_c\varepsilon_c^{pl}(1/b_c - 1) + \sigma_c} \tag{6}$$

$$d_t = 1 - \frac{\sigma_t l_0}{E_c w^{pl}(1/b_t - 1) + \sigma_t l_0} \tag{7}$$

where b_c is the ratio of plastic strain ε_c^{pl} to inelastic strain ε_c^{in},$b_c = \varepsilon_c^{pl}/\varepsilon_c^{in}$;

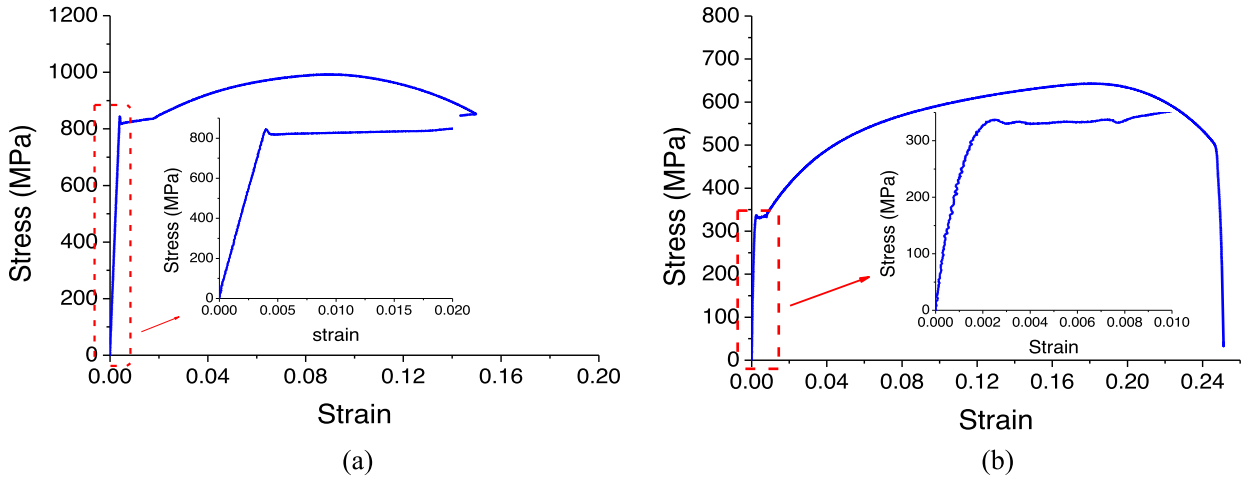

Fig. 7. Stress–strain relationship for (a) Bolt and (b) Tube.

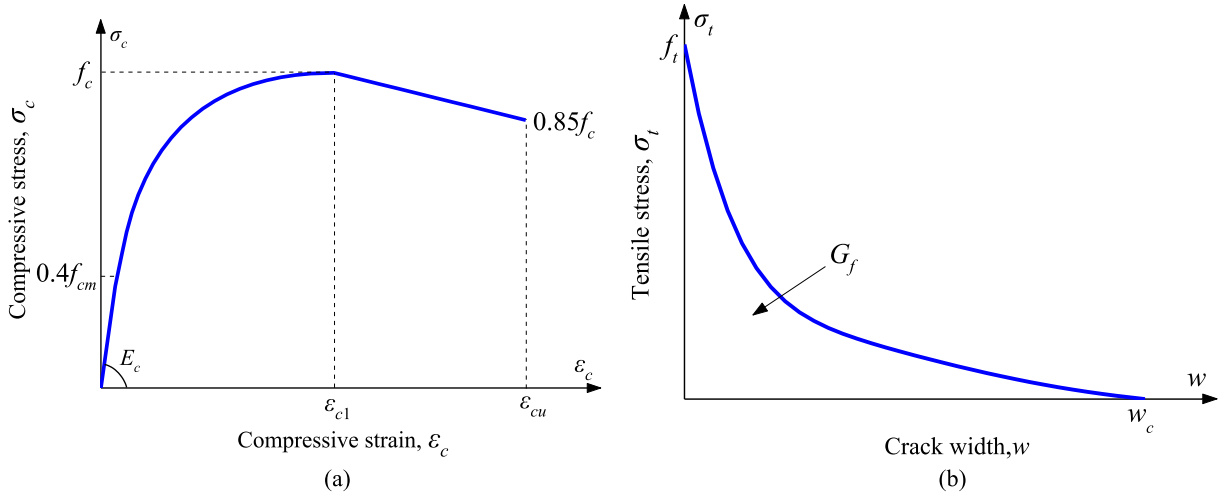

Fig. 8. Material stress strain law used for concrete and grout (a) in compression and (b) in tension.

and b_c is taken as 0.7, assuming that most of the inelastic compressive strain maintains after unloading; l_0 is assumed to be one-unit length; b_t is the ratio of the "plastic" crack width w^{pl} to the crack width w, $b_t = w_{pl}/w$, and b_t is set as 0.1, which means that the unloading returns almost back to the origin [57].

4. Experimental and FEM results

4.1. Failure modes

In the specimens where two connectors in each slab were installed, i.e. LB-DSC1, LB-DSC2 and LB-DSC3, bolt shear failure happened at the shank above the lug, where the stress reached the tensile strength at the ultimate state as shown from the FEM simulations in Fig. 9b and 10b. At the same time, a small amount of concrete in front of the fractured bolt was crushed; the plastic strain in the concrete at this local area was more than the ultimate compressive strain of concrete, as shown by the FEM model in Fig. 9c and 10c. The specimen with four LB-DSCs installed in each slab (LB-DSC4) failed unexpectedly due to cracking of the slab mainly at the bottom part as shown in Fig. 10d, and with extreme yielding of bolt's shank just above the lug but without fracture, as shown in Fig. 10e. The initiation and propagation of concrete cracks before the bolt fracture can be attributed to absence of gypsum plaster beneath the concrete slab as can be observed in Fig. 10a. In addition, the peak applied load was 1755 kN in this specimen, which means that the compressive stress in each slab was higher than the rest of the pushout tests.

4.2. Load-slip behaviour

Fig. 11 describes the load-slip behaviour of the specimens. A typical load-slip curve includes three main stages. The first stage is linear and involves elastic deformations, starting from 0.0 to 0.3–0.5 mm of slip, and matches to loads from 60 to 80 kN (i.e., about 33 % of shear resistance). The 25 loading cycles show that the difference in residual slip between two successive cycles approaches zero as the cycles approaches 25 which indicate that the current connector is reliable and not susceptible to premature or progressive failures. As the load increases, bolt bending, shearing and bearing against the surrounding grout and concrete result in reduction of LB-DSC stiffness, which leads to a nonlinear load-slip relationship which defines the second stage. After the maximum load, the slip increases rapidly, and the load capacity drops abruptly due to bolt shear failure just above the lug of the shank which defines the third stage. For the case of LB-DSC4 specimen, the stiffness reduction is due to, in addition to bolt's deformation, excessive cracks in the concrete slab. It is worth noting that the slip capacity of all

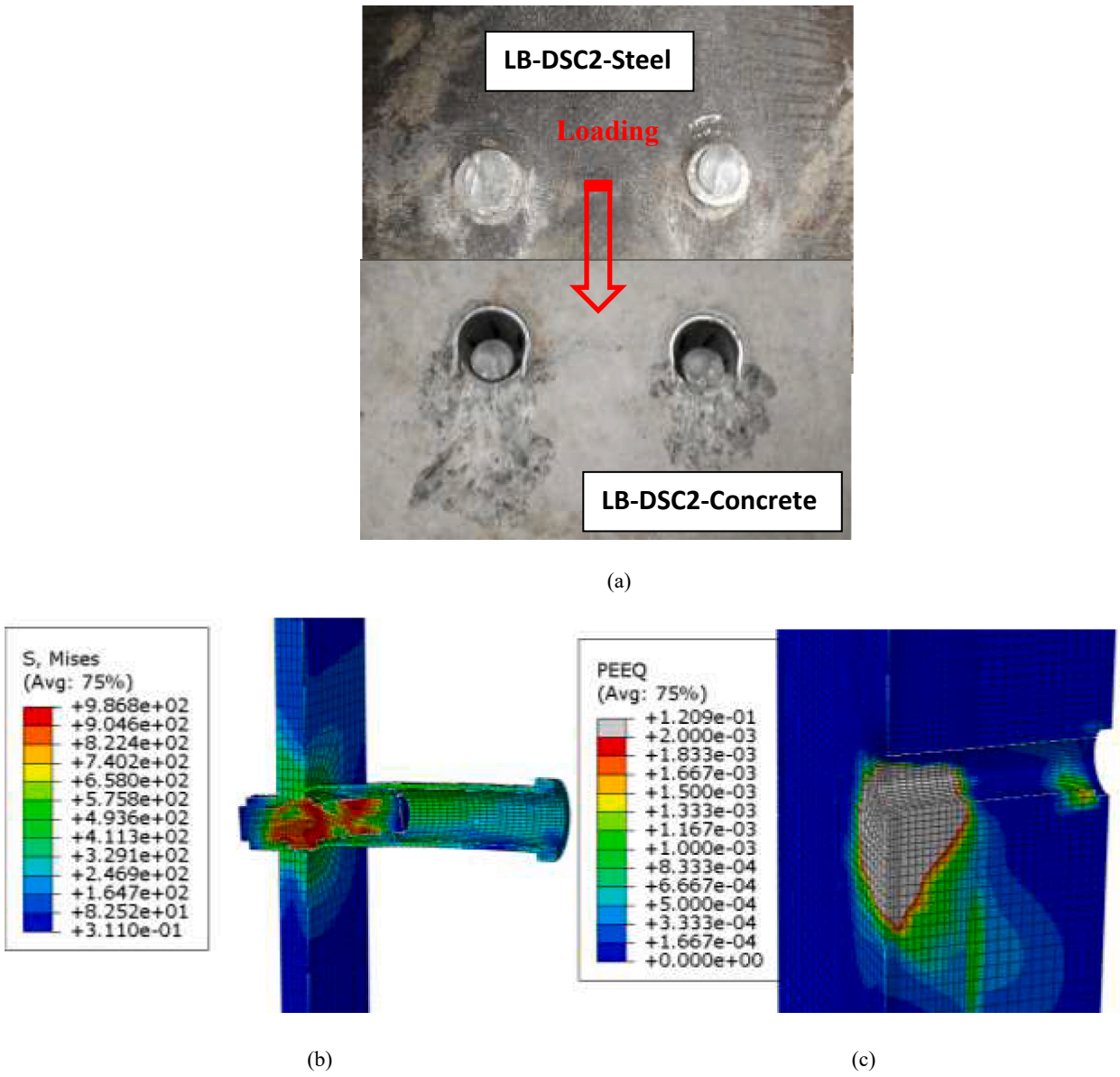

Fig. 9. Failure mode of Specimen LB-DSC2 without infill grout: (a) Bolt shear failure from test; (b) Mises stress of shear connectors at ultimate state from FEM; (c) PEEQ of concrete slab at ultimate state from FEM.

the specimens was more than 6 mm, which fulfils the Eurocode 4 requirement for ductile shear connectors. In addition, the validation of the FEM model was proved by noticing that FEM and experimental curves are in good agreement with each other, showing that the numerical model can capture all the stages of the load-slip responses with satisfactory agreement. Note that the effect of the 25 initial cycles of loading on the stiffness of the LBDSC was not considered in the FEM simulations.

Fig. 12 shows the load-separation relationships of all test specimens. It should be noted that the measured separation for LB-DSC1 was accidentally lost when the applied load was in between 60 and 208 kN. The separation capacity (defined as the measured separation at 80 % of the peak load) was recorded for all test specimens and the maximum was 0.51 mm or 18 % of the corresponding slip, which is below the limit of 50 % in Eurocode 4.

In addition, the mean value of the ratio of separation at ultimate load from the FEM model to that from pushout tests (except LBDSC4, since it failed due to concrete cracks, leading to large separation at failure) is 0.95, with a standard deviation of 0.08, implying that the numerical model was able to reliably calculate the separation of the LB-DSCs.

Recent pushout tests conducted by the authors in [50] assessed the behaviour of LB-DSCs using a horizontal setup of pushout test. The tests in [50] recorded values higher than 6 mm of the separation displacement at peak load, resulting in tension forces in bolts of the LB-DSCs up to 37 % of the shear resistance. This high value of tension indicated that tension-shear interaction may have compromised the shear resistance of the connectors in the horizontal setup pushout tests. Therefore, in the present standard pushout tests, the separation was also analysed using the FEM model and the results are shown in Fig. 13. The maximum tension force is 42 kN (except for LB-DSC4, for which it is 58 kN). Fig. 14 illustrates the relation between the tension force and the shear resistance. No matter whether the test specimen infilled with or without grout, the tension force resisted by the “hat” of the tube for LB-DSC1-3 is 13–15 % of the shear force. This ratio is less by about 50 % than that (23 % to 37 %) from horizontal pushout tests [50], and therefore the tension in the LB-DSC can be ignored. For specimen LB-DSC4 that failed due to

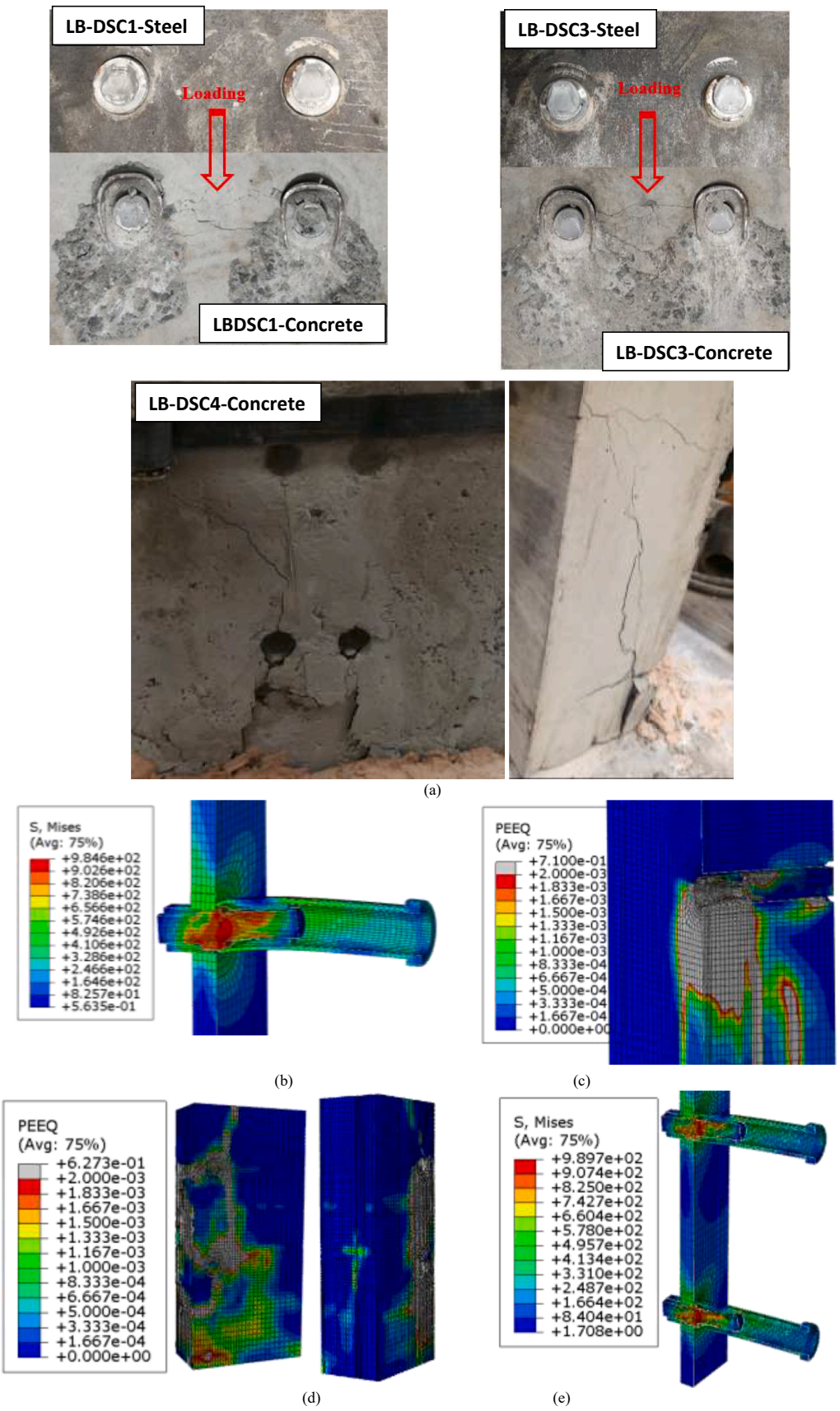

Fig. 10. (a) Failure mode of specimens LB-DSC1, 3 and 4 from tests; (b) Mises stress and (c) PEEQ at ultimate state of LBDSC3 from FEM; (d) PEEQ and (e) Mises stress at ultimate state of LBDSC4 from FEM.

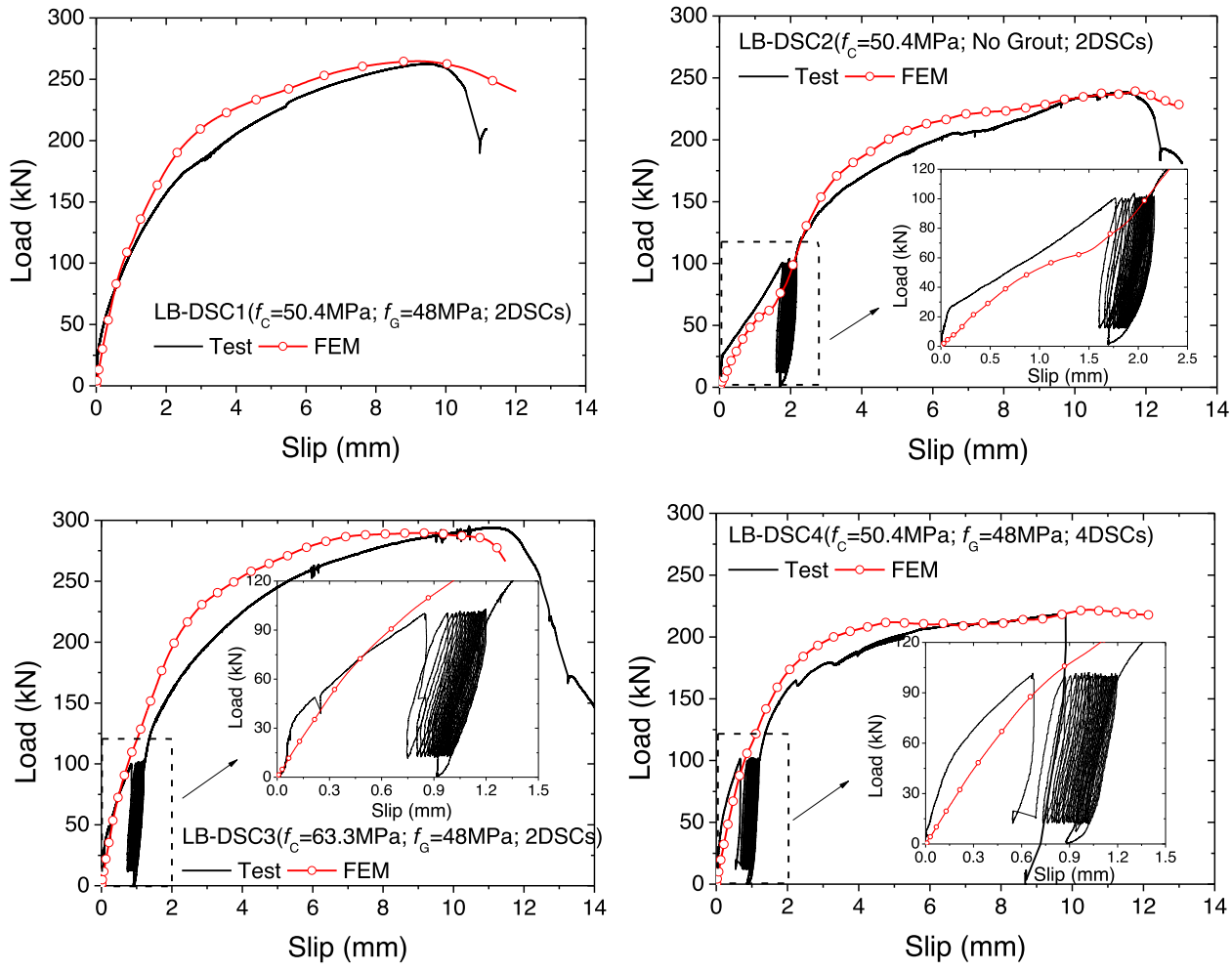

Fig. 11. Load versus slip responses.

concrete cracks, the ratio is slightly larger. Fig. 15 provides a comparison between the load-slip curves of specimen LBDSC1 (from the present standard pushout tests) and specimen LN9 (from the horizontal pushout tests presented in [50]). The two specimens have the same geometry of connector, while the strength of the concrete slab is slightly different: LB-DSC1 has 50 MPa, while LN9 has 37 MPa. It can be observed that the shear stiffness is almost the same, whilst the shear resistance of LB-DSC1 is higher than that of LN9 by 23 %. The slip capacity of LB-DSC1 is 10.9 mm which is less than that of LN9 by 148 %. The higher slip capacity in LN9 is attributed to a large rotation that occurred in the connectors of the horizontal setup tests due to the secondary moments induced from the eccentricity [50], and thus it is not representative of the slip capacity of the proposed connector in a composite beam. Therefore, the standard pushout tests presented in this paper are used to propose more reliable design equations to predict the shear resistance of the LB-DSC.

4.3. Shear resistance, ductility, and stiffness of the LB-DSC

Table 3 shows the results from both pushout tests and the numerical simulations including shear stiffness k, shear resistance F_u, corresponding slip S_u, slip capacity S_P, residual slip S_R after 25 load cycles, and separation capacity U_p. The shear stiffness is adopted as the secant line at $F_u/3$ of load-slip curve, since the curve is almost linear until that load.

The average ratios of numerical to experimental shear stiffness, shear resistance and corresponding slip are 0.95, 1.00 and 0.97, with standard deviations of 0.03, 0.02 and 0.06, respectively, indicating the FEM can reliably estimates the behaviour of the LB-DSC.

To evaluate the presence of infill grout on the structural performance, LB-DSC2 is compared to LB-DSC1 in Fig. 16a. The grout of 48 MPa compressive strength improved the shear resistance by 10 % and the stiffness by 230 %; hence, a significant enhancement in LB-DSC stiffness can be achieved with the presence of the infill grout and, to a lesser amount, in the shear resistance. Evaluation of the effect of concrete compressive strength was done by comparing LB-DSC1 (50.4 MPa) to LB-DSC3 (63.3 MPa) as shown in Fig. 16b. The shear resistance and stiffness improved by 12 % and 11 %, respectively, thus, increasing concrete strength of the slab can slightly improve the structural performance. In terms of the effect of number of bolts, when it was increased from 2 per slab in LB-DSC1 to 4 per slab in LB-DSC4 (Fig. 16c), the experimental shear resistance per bolt was reduced by 16 %, while the shear stiffness per bolt was increased by 13 %; therefore, a group effect similar to that for welded shear studs [20] and bolt connectors [58] is also observed for the LB-DSCs. A possible explanation to the 16 % reduction in shear resistance is that the specimen LB-DSC4 failed unexpectedly due to cracking of the slab mainly at the bottom part as shown in Fig. 10d as explained before in Section 4.1.

4.4. Comparison with recent DSCs

Fig. 17 shows a comparison of the load-slip relationships of the LBDSC, threaded studs (M9), bolts (M10) [59], blind bolts (B1-Lindapter

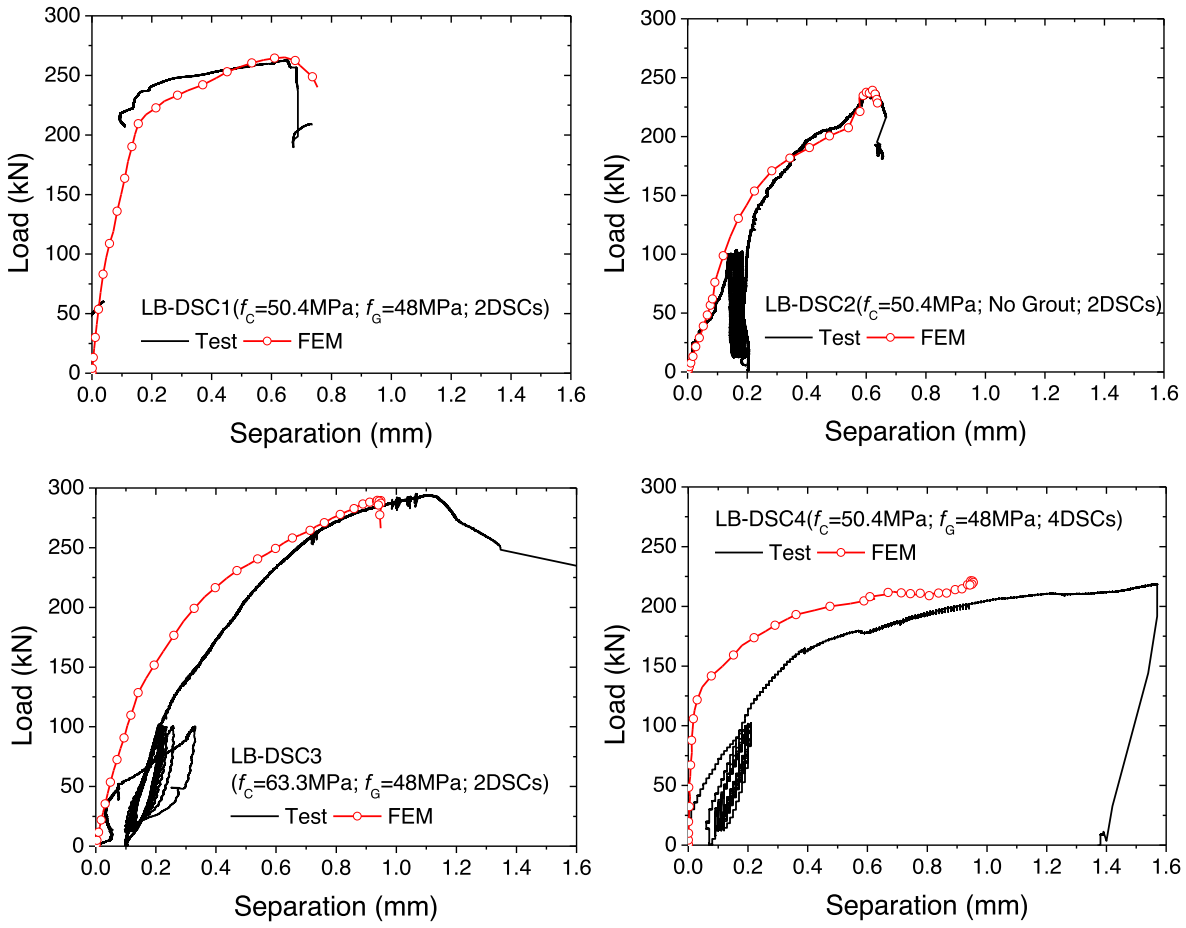

Fig. 12. Load versus separation responses.

Hollo-Bolt; B2: Ajax Bolt) [60], friction bolts with cast-in cylinders (*P*3.1), embedded mechanical coupler device with pre-tensioned bolts (P15.1) or with injection bolts (P15.2) [44], embedded bolts (M3) [31], embedded bolts with coupler (B9) [32], high-tension friction grip bolts (T1-4) [61], and locking-nut LNDSC (test 10) [62]. Table 4 lists the characteristics of geometry and material of the aforementioned DSCs, in addition to the failure mode, shear resistance, slip capacity, and normalized resistance, defined as the ratio *R* of tested shear resistance (Q_u) to tensile resistance ($f_u(\pi D^2/4)$ of the bolt for comparison of DSCs with different diameter and tensile strength.

The curves shown in Fig. 17 are further categorised according to the failure mode, i.e. bolt fracture (Fig. 17a) or concrete failure (Fig. 17b). The comparison reveals that both the shear resistance and the initial stiffness of the LB-DSC are the highest among the bolted DCSs regardless of the failure mode. In addition, the LB-DSC has competitive slip capacity in comparison to friction bolts and the LNDSC, but pretension is not required to be applied to the LB-DSC. The "locking" mechanism of the bolt into the counter-sunk hole in the steel flange effectively prevents the sudden slip of the bolt inside the hole due to the exceedance of the frictional resistance, resulting in higher initial stiffness of the LB-DSC as compared to the majority of other bolted DSCs.

5. Parametric study

The calibrated FEM model was adopted to conduct a parametric study to investigate the effects of several parameters on the structural performance of the LB-DSC. The investigated parameters include the bolt diameter, tube thickness, tube tensile strength, slab concrete compressive strength, infilled grout compressive strength, and bolt tensile strength on the LBDSC shear behaviour. The values of the default (base) parameters are: bolt diameter = 20 mm; bolt tensile strength = 990 MPa; tensile strength of tube = 645 MPa, thickness of tube = 2.5 mm; concrete compressive strength = 15 or 50 MPa, and compressive strength of grout = 45 MPa.

5.1. Compressive strength of concrete slab

To understand the influence of concrete compressive strength of the slab on the LB-DSC shear resistance and stiffness, the compressive strength of the slab was chosen as 15, 30, 40, 50 and 60 MPa, while the other parameters were kept constant. The corresponding load versus slip curves shown in Fig. 18 show that the shear stiffness ascends almost linearly, and the shear resistance ascends nonlinearly when the compressive strength of the concrete slab ascends from 15 N/mm^2 to 60 N/mm^2. The increments are 30 % and 24 % for shear resistance and stiffness respectively, indicating that increasing compressive strength of concrete can enhance the performance of the LB-DSC. In addition, it is shown that the increase in compressive strength is insignificant for concrete strength greater than 30 MPa, since the failure mode converted from concrete cracking to bolt shearing-off.

5.2. Thickness of tube

The variation of thicknesses of steel tube was 2, 2.5 and 3 mm and it was considered in both specimens with low compressive strength of concrete slab (15 MPa) and with high strength (50 MPa), as shown in

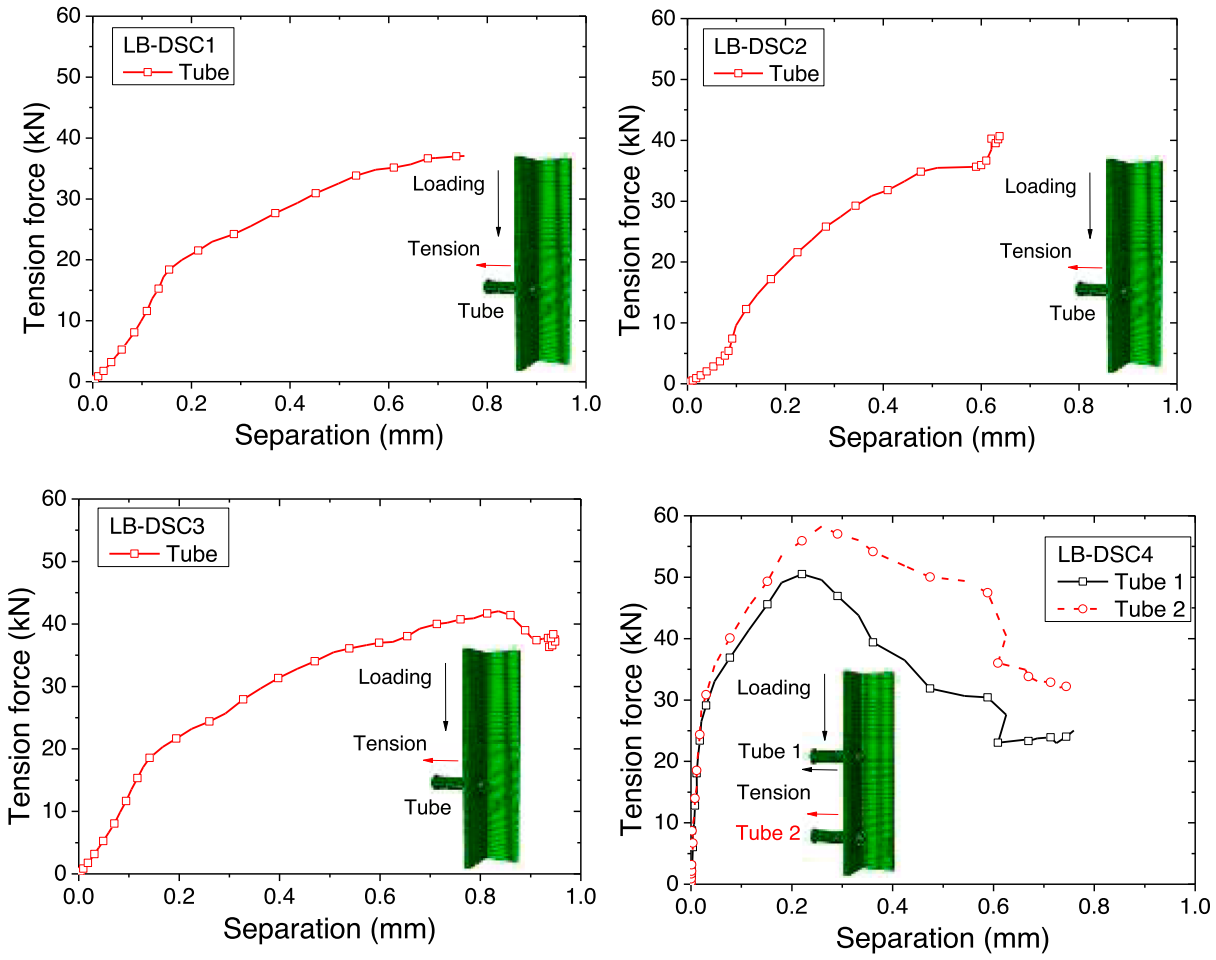

Fig. 13. Tension force versus separation for test specimens.

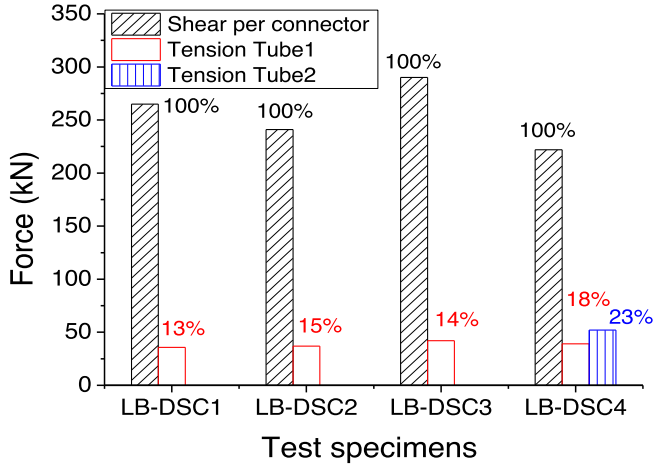

Fig. 14. The relation of shear and tension force at ultimate state from FEM.

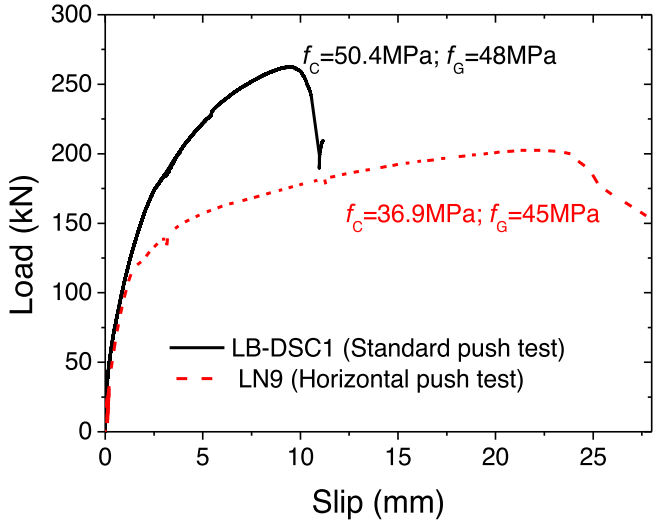

Fig. 15. The comparison of load-slip curves between standard and horizontal push tests for LBDSC.

Fig. 19. Increases of 18 % and 5 % in the shear resistance were recorded as the thickness changes from 2 to 3 mm for low and high strength concrete slab, respectively. The shear stiffness almost keeps the same (5 % variation). Thus, using thicker steel tubes guarantees higher shear resistance of the LB-DSC when it is embedded in low strength concrete slab, whilst the effect is insignificant in high strength concrete slab.

5.3. *Tensile strength of tube*

Different tube tensile strengths ranging from 400 to 700 MPa were considered in models with slab concrete compressive strength of 15 MPa and 50 MPa respectively. Fig. 20 shows the corresponding load-slip

Table 3
Comparison of experimental and numerical results.

Specimen	Shear resistance F_u (kN)			Slip at F_u S_u(mm)			Slip capacity S_p (mm)	Residual slip S_R (mm)	Separation capacity U_p (mm)	Stiffness at 1/3 F_u k (kN/mm)			Failure mode
	Test	FEM	FEM /Test	Test	FEM	FEM /Test	Test	Test	Test	Test	FEM	FEM /Test	
LB-DSC1	263	265.1	1.01	9.42	9.10	0.97	10.9	–	0.10	141	139	0.99	Bolt shear off
LB-DSC 2	239	239.3	1.00	11.35	10.75	0.95	12.7	1.70	0.39	61	57	0.93	Bolt shear off
LB-DSC 3	295	287.6	0.97	10.43	9.44	0.91	12.6	0.92	0.62	157	152	0.97	Bolt shear off
LB-DSC 4	219	222.4	1.01	9.82	10.40	1.06	9.8	0.88	0.51	160	147	0.92	Concrete crush and split
Average	254		1.00			0.97	11.5			153*		0.95	
Standard deviation			0.02			0.06						0.03	

* Specimens with grout-infilled tube.

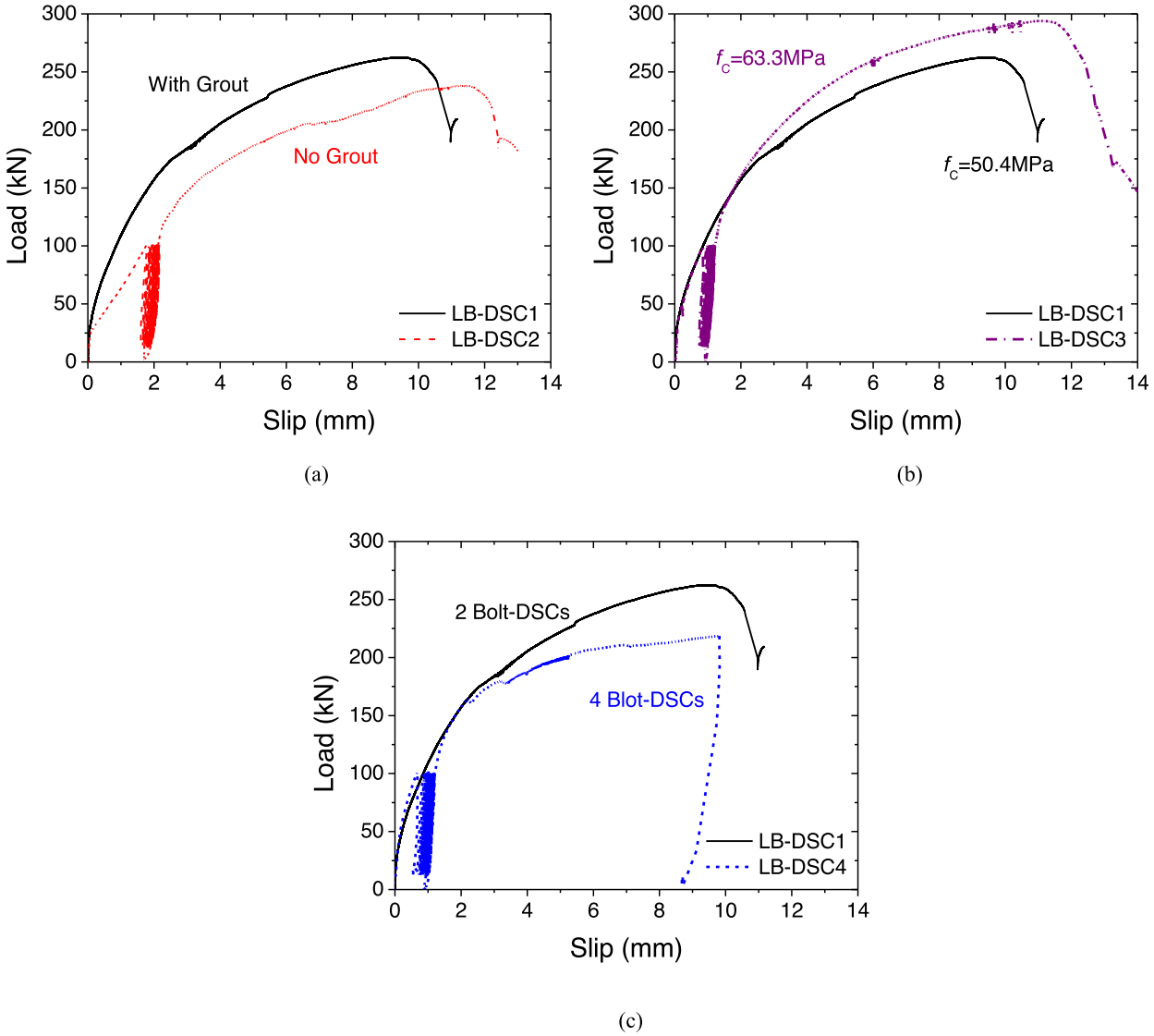

Fig. 16. Comparison of load-slip curves for test specimens: (a) with or without grout; (b) with different strength of concrete slab; (c) with different connector number.

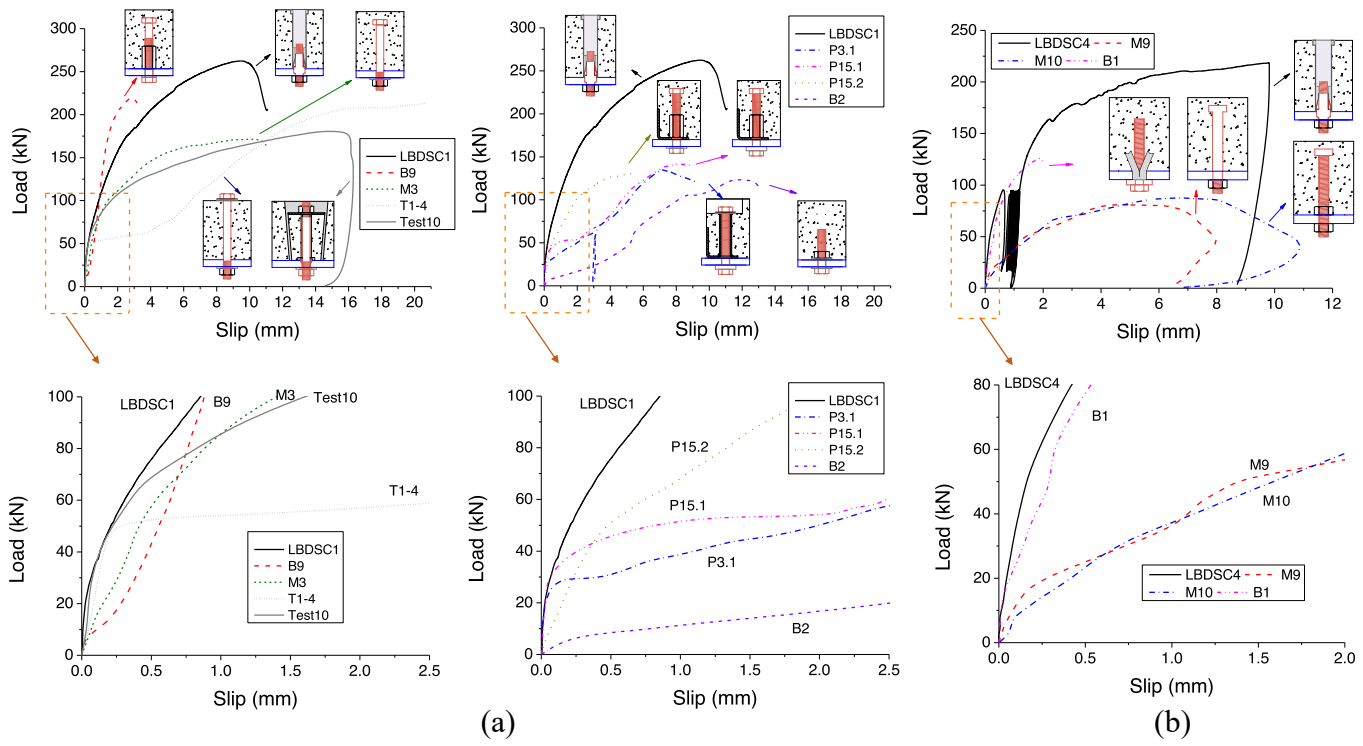

Fig. 17. Comparison of load-slip curves for bolt DSCs: due to (a) Bolt fracture failure; (b) Concrete failure.

Table 4
Comparison of LBDSC with other bolt DSCs.

Specimens	Bolt diameter D (mm)	Bolt tensile strength f_u (MPa)	Concrete slab strength f_c (MPa)	Pretension T (kN)	Shear resistance Q_u (kN)	$R = Q_u/f_u(\pi D^2/4)$	Slip capacity	Failure mode
LB-DSC1	20	990	50.4		262.6	0.84	10.9	BF
LB-DSC4	20	990	50.4		219.4	0.71	9.8	CF
B9	22	985.6	48.9		219	0.58	3.37	BF
P3.1	20	948.7	59.4	100	136	0.46	9.4	BF
P15.1	20	948.7	44.3	176	142	0.48	9.0	BF
P15.2	20	948.7	44.3	0	131	0.44	5.6	BF
M3	20	925	52.2		171	0.59	11	BF
T1-4	20	1150	50	155	213	0.59	20.7	BF
M9	20	510	50.8		80	0.50	6.1	CF
M10	20	768.8	51.3		87	0.36	7.9	CF
B1	20	920	42		126	0.44	1.9	CF
B2	20	900	42		123	0.44	11.6	BF
Test10	16	889	43	88–106	181	1.01	16.2	BF

Note: BF: bolt fracture failure; CF: concrete failure.

curves. The shear resistance was improved by 16 % and 6 % for specimens with low and high strength slab respectively, as the tensile strength increases from 400 MPa to 700 MPa. The shear stiffness practically did not change for all specimens (6 % variation). Therefore, using steel tube of high tensile strength lightly improves the shear resistance of the LB-DSC embedded in low compressive strength concrete slab, whilst the effect is insignificant for connectors embedded in high strength slabs.

5.4. Compressive strength of in-filled grout

Fig. 21 depicts the effect of the infilled grout in the tube, and its compressive strength considering the values of 30, 45 and 60 MPa, on the performance of the LB-DSC. The infilled grout can considerably improve the stiffness by up to 240 % with respect to no grout-infilled connectors. Additionally, the infilled grout can increase the shear resistance by 12 % and 20 % in LB-DSCs with high and low strength concrete slabs, respectively. Since the bolt was confined by infilled grout, both the stiffness and the resistance of the LB-DSC were improved, especially in specimens with bolt fracture failure. Fig. 21 shows that the effect of compressive strength of the infilled grout results in minor enhancements in shear resistance and stiffness of the LB-DSC. Therefore, the steel tube should be filled with grout, but the compressive strength of the in-filled grout is not important as long as it is beyond 30 MPa.

5.5. Bolt's diameter

Fig. 22 shows the effect of varying bolt's diameter as follows (16, 20, 22 and 25 mm) on the shear resistance and stiffness, for low and high compressive strength concrete slabs. It should be noted that the inner diameter of the steel tube was changed to 26, 30, 32, and 35 mm, accordingly, to ensure that the bolt's base is confined by the grout. It can

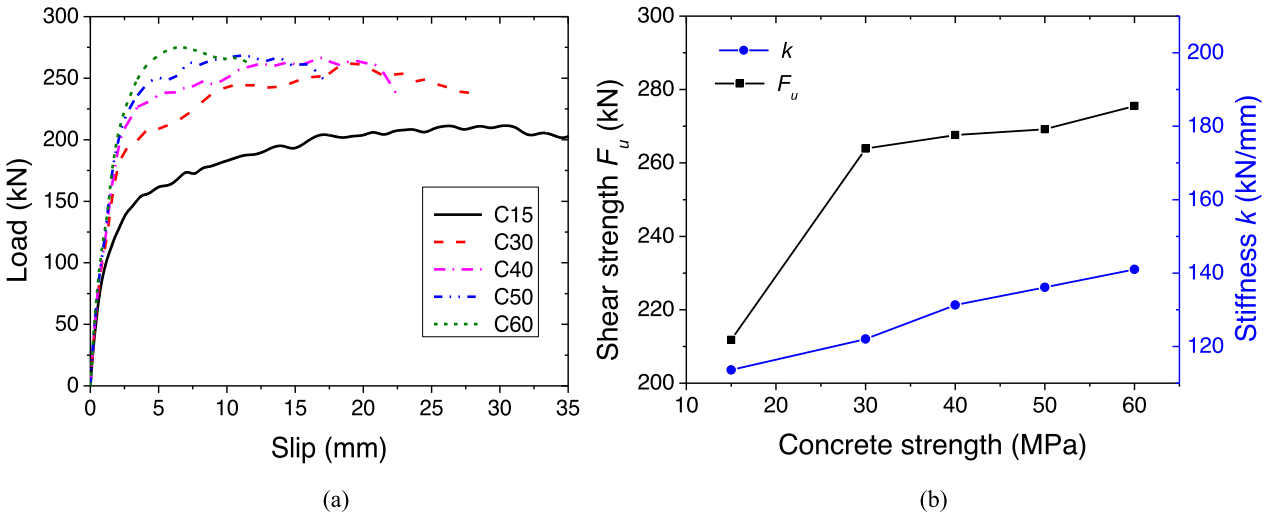

(a) (b)

Fig. 18. Effect of concrete slab strength: (a) load-slip curves; (b) Relation between shear strength, stiffness and concrete strength of the slab.

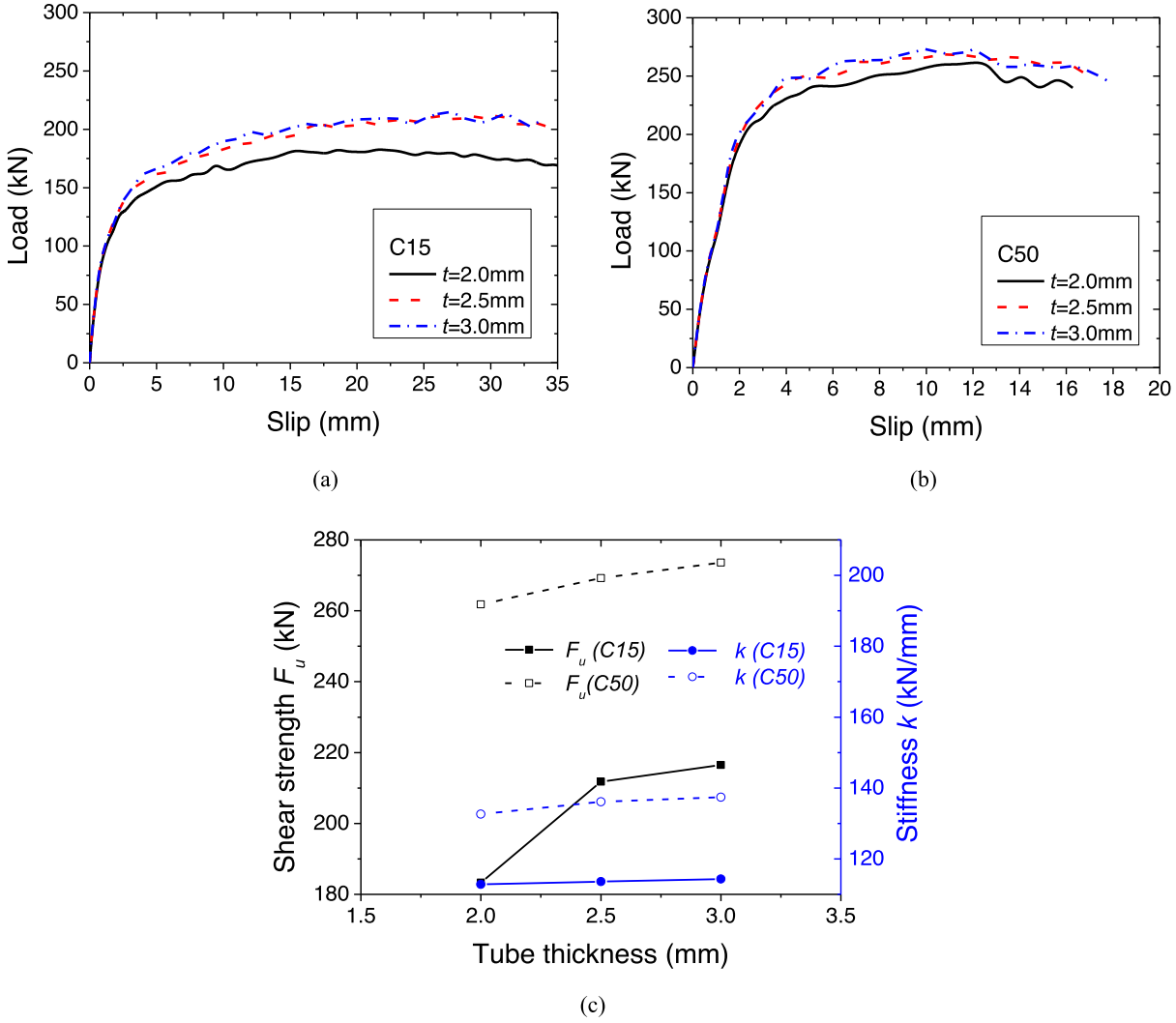

(a) (b)

(c)

Fig. 19. Effect of steel tube thickness: load-slip curves for specimens with concrete slab of (a) 15 MPa and (b) 50 MPa; (c) Relation between shear strength, stiffness and steel tube thickness.

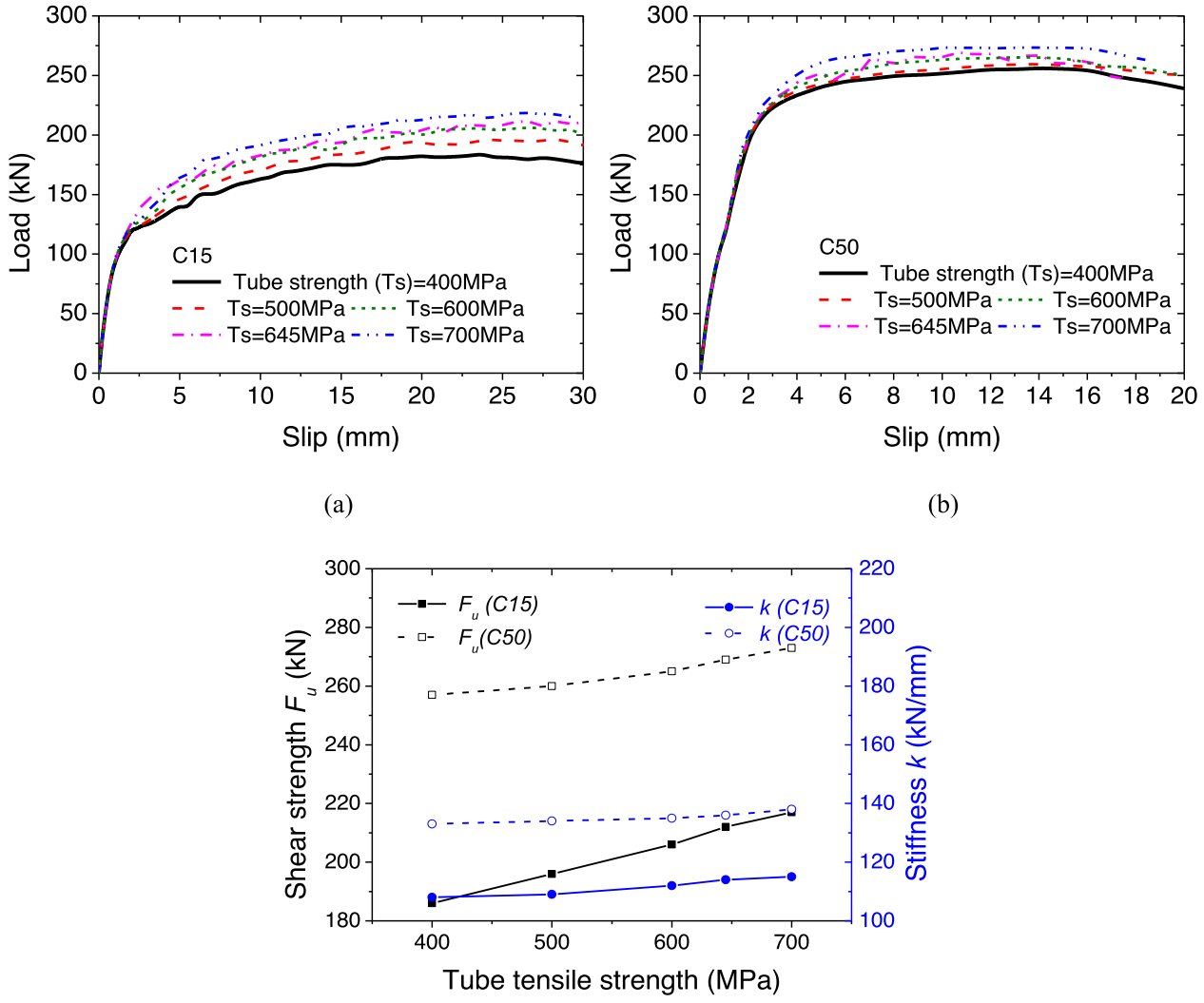

Fig. 20. Effect of tube tensile strength: load-slip curves for specimens with concrete slab of (a) 15 MPa and (b) 50 MPa; (c) Relation between shear strength, stiffness and tube tensile strength.

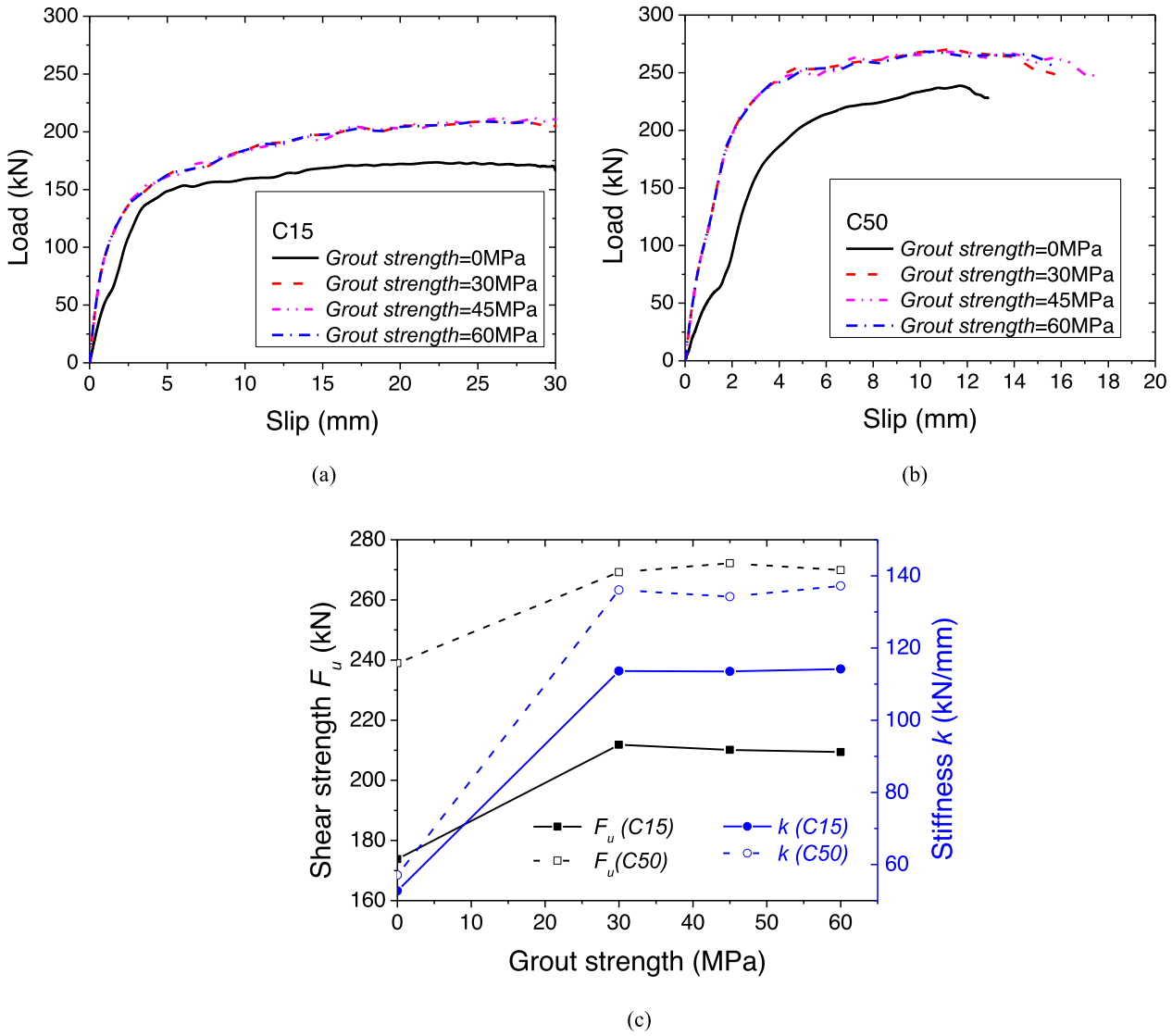

Fig. 21. Effect of infilled grout: load-slip curves for specimens with concrete slab of (a) 15 MPa and (b) 50 MPa; (c) Relation between shear strength, stiffness and infilled grout strength.

be found that both the shear resistance and stiffness increase nonlinearly as the bolt diameter increases. The increments in shear resistance and stiffness are about 50 % and 35 % respectively when the bolt diameter changes from 16 mm to 25 mm. Therefore, using bolts with large diameters can significantly enhance the shear resistance and stiffness of the LB-DSC.

5.6. Bolt's tensile strength

Fig. 23 shows the influence of bolt tensile strength (800, 990, and 1100 MPa for Bolt 6.8, 8.8 and 10.9) on the shear resistance and stiffness of the LB-DSC, in low and high compressive strength concrete slabs. The shear resistance rises almost linearly with the increasing of the bolt tensile strength, and the increasing ratio of the specimens with high compressive strength slab (31 %) is larger than that of the specimens with low compressive strength slab (13 %) when the tensile strength of bolt of 800 MPa enlarged to 1100 MPa. However, the stiffness almost remains unaffected with only 3 % variation. Thus, increasing bolt tensile strength can increases the shear resistance but does not influence the stiffness of the LB-DSC.

6. Design rules for the shear resistance of the LBDSC

The shear resistance of headed studs in steel–concrete beams is dictated by either fracture of the stud or cracking of the concrete slab. Therefore, various design codes provide formulas to estimate the shear resistance based on the minimum of the two failure modes. The design equations pertaining to welded headed studs prescribed in the Eurocode 4 [51], AISC360-10 [63], *ACI* 318-08 [64], GB50017 [65], AASHTO [66] are summarised in Table 5.

Currently, the design shear resistance of the LB-DSC is not included in design codes. Based on the code-based shear resistance prediction expressions in Table 5 for headed studs, the following equation is proposed to estimate the shear resistance of the LB-DSC:

$$P_u = \min\left(\alpha_1 A_t \sqrt{E_c f_c'},\quad \alpha_2 A_s f_u\right) \tag{8}$$

where, P_u is shear resistance; A_s is cross-sectional area of the bolt shank; A_t is cross-sectional area of grout-infilled tube; f_c' is cylindrical compressive strength of concrete; f_u is tensile strength of the bolt, and E_c is Young's modulus of the concrete; α_1 and α_2 are factors for considering

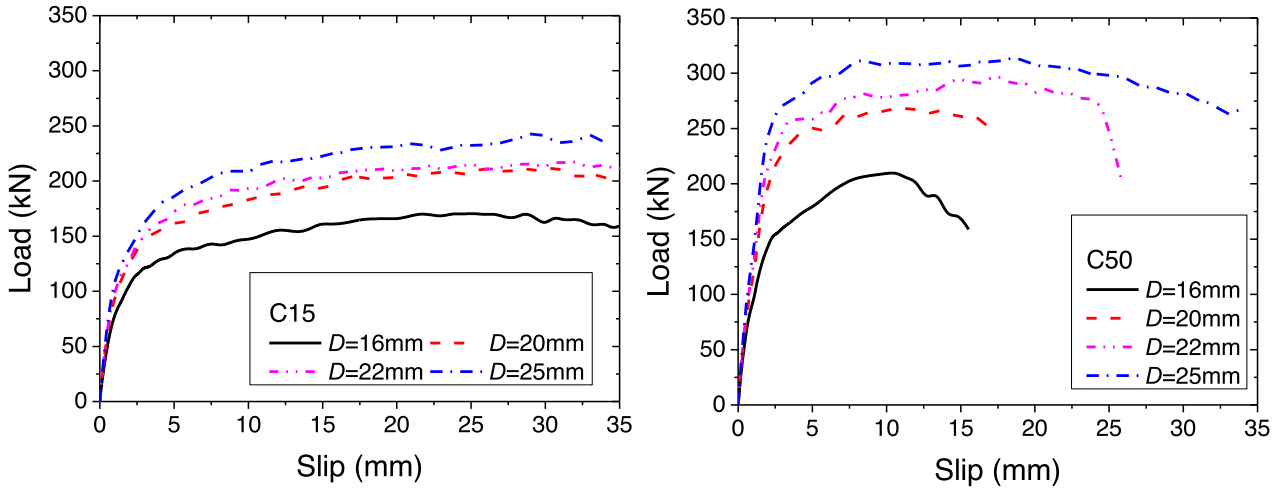

(a) (b)

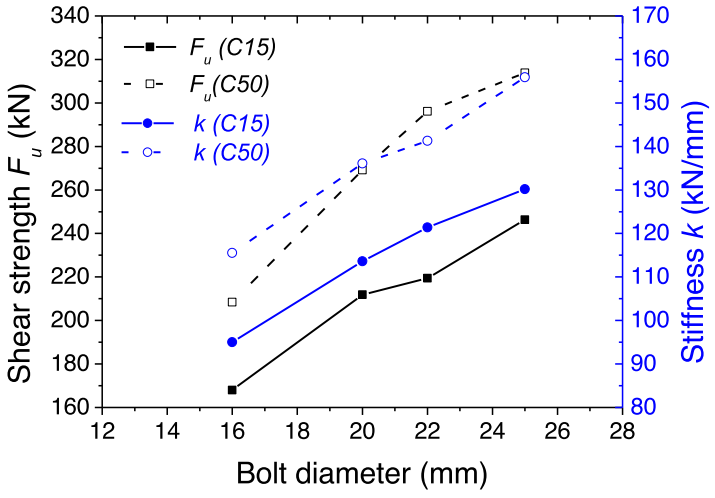

(c)

Fig. 22. Effect of bolt diameter: load-slip curves for specimens with concrete slab of (a) 15 MPa and (b) 50 MPa; (c) Relation between shear strength, stiffness and bolt diameter.

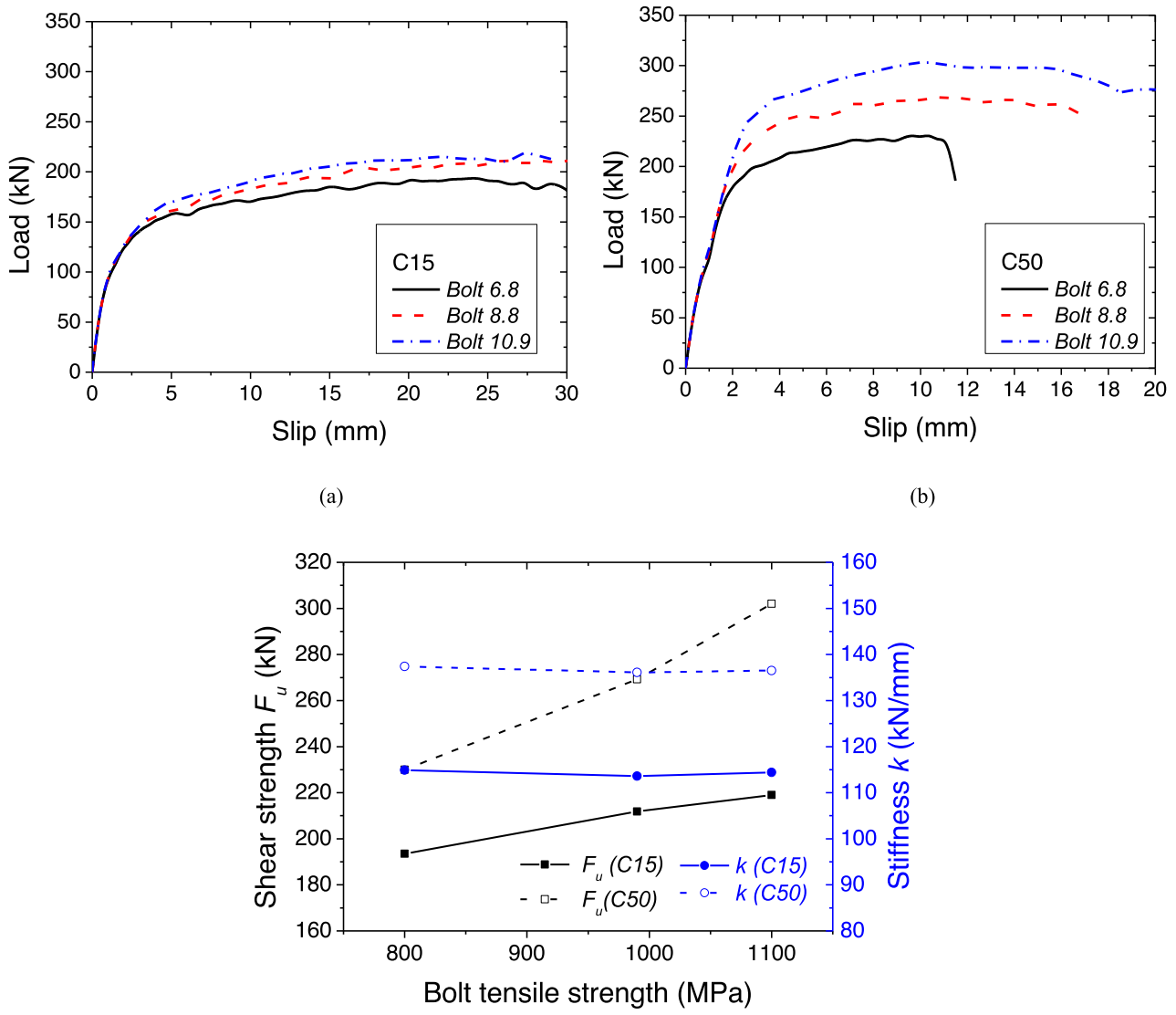

Fig. 23. Effect of bolt tensile strength: load-slip curves for specimens with a concrete slab of (a) 15 MPa and (b) 50 MPa; (c) Relation between shear strength, stiffness and bolt tensile strength.

Table 5
Code-based calculation of the shear strength for headed stud connectors.

Code	Expression
Eurocode 4	$P_u = 0.29\alpha d^2\sqrt{E_c f_c'}/\gamma_v \leqslant 0.8A_s f_u/\gamma_v$; $\alpha = 0.2\left(\frac{h_{sc}}{d}+1\right)$ for $3 \leqslant \frac{h_{sc}}{d} \leqslant 4$; $\alpha = 1$ for $\frac{h_{sc}}{d} > 4$
AISC360-10	$P_u = 0.5A_s\sqrt{E_c f_c'} \leqslant R_g R_p A_s f_u$
ACI 318–08	$P_u = k_{cp}k\sqrt{f_c'}h_{ef}^{1.5} \leqslant \varphi A_s f_u$
AASHTO	$P_u = \phi_{sc}0.5A_s\sqrt{E_c f_c'} \leqslant \phi_{sc}A_s f_u$
GB50017	$P_u = 0.43A_s\sqrt{E_c f_c} \leqslant 0.7\gamma A_s f_u$

NOTE: P_u: shear resistance of headed studs; A_s: cross-sectional area of stud shank; f_c' and f_c: specified and allowable cylinder compressive strength of concrete, respectively; f_u: tensile strength of studs; E_c: Young's modulus of concrete; d: diameter of the studs; h_{sc}: height of the stud; R_g, R_p, φ, φ_{sc}, γ: partial safety factors specified in codes.

concrete cracking failure and bolt fracture, respectively, and are depicted in Fig. 24, in which the mean value of α_1 is almost constant for bolt diameter 16–25 mm, and α_2 decreases as bolt diameter (d) increases. Thus, for concrete failure, the value of α_1 is fitted as a constant of 0.30. As for the factor α_2, there are several recommendations in the literature for bolts. Eurocode 3 [67] prescribes the values of $\alpha_2 = 0.6$, for bolt classes 4.6, 5.6, 8.8, and $\alpha_2 = 0.5$, for bolt classes 4.8, 5.8, 6.8, 10.9, when shear plane passes through the threaded portion of the bolt. To calculate the ultimate strength of post-installed shear connectors, $\alpha_2 = 0.5$ was suggested [25]. And $\alpha_2 = 0.54$ was recommend [58] for multiple M16 bolt connectors in prefabricated concrete slab considering group effect of bolt connectors. To predict the shear resistance of the high-strength friction-grip bolt (HSFGB), α_2 was modified to 0.66 [29]. Based on pushout out tests on assembly of shear connectors, α_2 was determined to be 0.8 [32]. However, from extensive numerical parametric analyses [27], it was found that α_2 decreases with further increase of bolt diameter and the relation of α_2 and diameter ratio (d_{ref}/d) can be expressed as power law function. Therefore, the factor α_2 should consider the effect of diameter in Eq. (8) for bolt failure, which can be

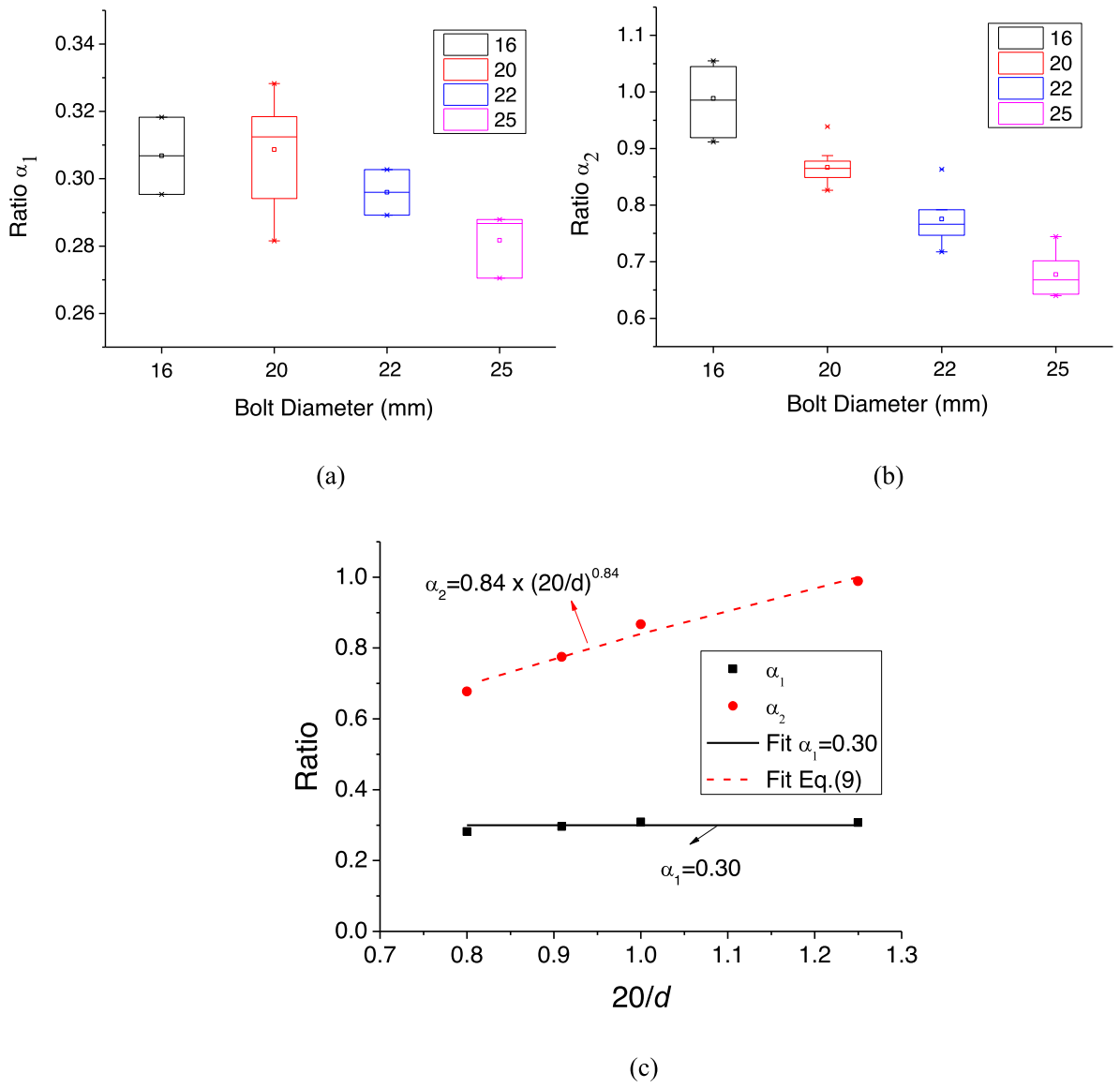

Fig. 24. The determination of the ratio: (a) α_1; (b) α_2; and (c) fitted curves.

expressed as follows:

$$\alpha_2 = \alpha_b \left(\frac{d_{ref}}{d}\right)^{\beta} \leqslant 1 \; for \; d \geqslant 16 \; mm \tag{9}$$

where d_{ref} is representing a reference bolt diameter, $d_{ref} = 20$ mm in the present study, α_b is the shear resistance factor for the bolts with reference diameter, while the exponent β is used to account for the sensitivity of the diameter variation. Thus, for bolt fracture failure, the value of α_b and β are fitted as 0.84 and 0.84, respectively.

Fig. 25 compares the shear resistance of the LBDSC predicted by Eqs. (8) and (9) (P_{u_cal}) to those obtained from FEM ($P_{u\_FEM.}$) and pushout test (P_{u_test}). The average ratio of P_{u_cal} / P_{u_FEM} is 0.995, with a standard deviation of 0.05, while average ratio of P_{u_cal} / P_{u_test} is 1.04, with a standard deviation of 0.13, indicating that Eq. (8) can predict the shear resistance of LB-DSC with acceptable accuracy. It should be noted that the use of the proposed parameter (α_2) is limited to high strength bolts with diameter d ≥ 16 mm, because a larger factor α_2 would be obtained for smaller bolt diameters. Moreover, bolts with diameter smaller than 16 mm are not recommended in the proposed LB-DSCs for application in large span steel–concrete structures.

7. Conclusions

A lockbolt demountable shear connector (denoted as LB-DSC) is proposed in this paper for application in sustainable steel–concrete structures. The LB-DSC was assessed experimentally through four Eurocode 4 pushout tests. A nonlinear numerical model using Abaqus was also calibrated through comparison with experimental results and then used to conduct a parametric study. On the basis of the experimental and numerical results, the following conclusions can be obtained:

- The experimental and numerical results indicate that the LB-DSC with the geometry presented in this paper has high shear resistance (254 kN in average), high stiffness (higher than most DSCs), and slip capacity much higher than the 6 mm required by Eurocode 4 (11.5 mm in average). Thus, the LB-DSC can provide an effective shear connection between a steel section and the concrete slab in a steel–concrete composite beams and could be used in composite beams with partial shear connection.
- The lockbolt geometry effectively prevents sudden slip before SLS resulting in high initial stiffness. This is clearly demonstrated in the

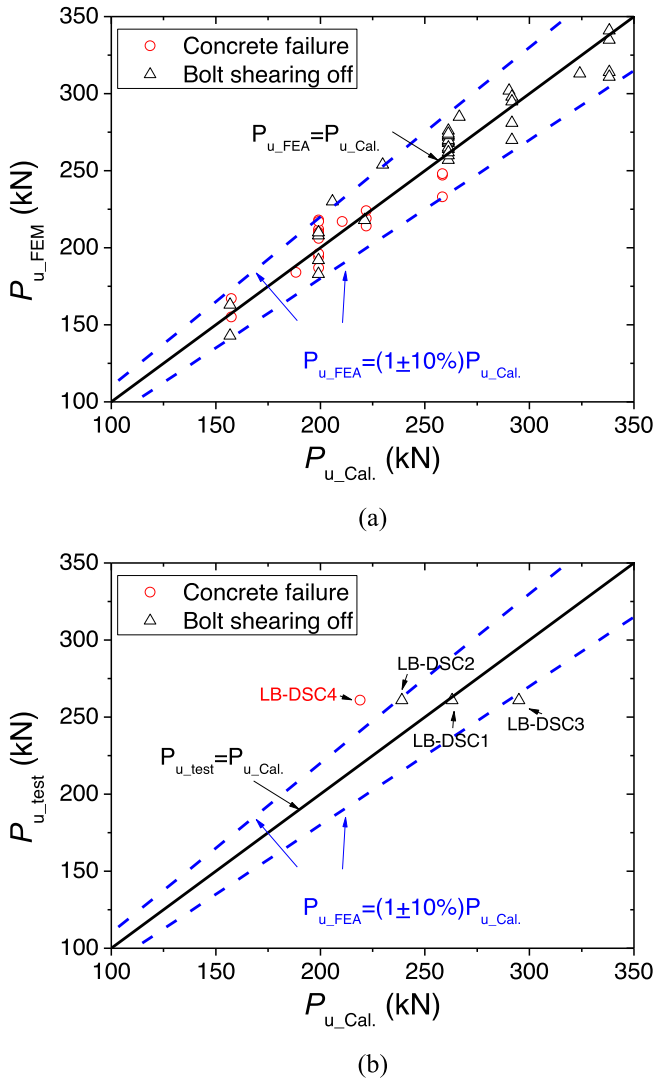

Fig. 25. The comparison of predicted and (a) FEM analytical (b) tested shear strength.

comparisons with previous bolted DSCs. In addition, it renders the connector less sensitive to construction tolerances.

- The LBDSCs with or without infilled grout exhibited ductile shear failure including fracture of bolt shank and local crushing of concrete.
- The infilled grout in the steel tube results in a significant increase in the initial stiffness of the LBDSC, and it has an insignificant effect on its shear resistance. In addition, the compressive strength of the grout does not affect the shear resistance considerably. Therefore, grouting the tube without special consideration of the grout strength is allowed.
- The standard pushout tests presented in this study revealed a difference with recent horizontal setup pushout tests on the same connector and highlighted the importance of test setup. The separation capacity in the present tests only accounts for 3–18 % of the corresponding slip, and the separation induced tension force is less than 15 % of the applied shear force, which can be ignored.
- Increasing slab concrete compressive strength and tube thickness can enhance shear stiffness and resistance to a moderate degree, while increasing bolt diameter can significantly improve the shear resistance and stiffness. On the other hand, only shear resistance can be obviously improved as the increasing of bolt tensile strength, especially when LB-DSC is embedded in high compressive strength concrete slab.
- The shear resistance of the LB-DSC can be reliably predicted by the proposed design equations with calibrated parameters according to the numerical and experimental results, provided that high strength bolt with a diameter of at least 16 mm is used.

Declaration of Competing Interest

The authors declare that they have no known competing financial interests or personal relationships that could have appeared to influence the work reported in this paper.

Acknowledgments

The authors wish to express their gratitude to the financial support provided by Horizon 2020 - Marie Skłodowska - Curie Individual Fellowship of European Commission (REUSE: 793787), the National Nature Science Foundations of China (51978081, 5211101838), and the Natural Science Foundation of Hunan Province, China (2021JJ30712, 2022JJ10049). The authors are grateful to the technicians at the Heavy Structures Lab at Heriot-Watt University, Edinburgh, UK.

References

[1] Hardy A. State of the Nation 2020: Infrastructure and the 2050 net-zero target. Institution of Civil Engineers; 2021 (n.d.). https://www.ice.org.uk/news-and-insight/policy/son-2020-infrastructure-and-2050-net-zero-target (accessed April 27, 2021).
[2] Galvin R, Healy N. The Green New Deal in the United States: what it is and how to pay for it. Energy Res Social Sci 2020;67:101529.
[3] Arsova S, Corpakis D, Genovese A, Ketikidis PH. The EU green deal: spreading or concentrating prosperity? Resour Conserv Recycl 2021;171(1):105637.
[4] IEA (International Energy Association). Tracking Industrial Energy Efficiency and CO_2 Emissions. Paris: IEA; 2007.
[5] Brambilla G, Lavagna M, Vasdravellis G, Castiglioni CA. Environmental benefits arising from demountable steel-concrete composite floor systems in buildings. Res Conserv Recycl 2019;141(2):133–42.
[6] Brozzetti J. Design development of steel-concrete composite bridges in France. J Constr Steel Res 2000;55(1–3):229–43.
[7] Galambos TV. Recent research and design developments in steel and composite steel-concrete structures in USA. J Constr Steel Res 2000;55(1–3):289–303.
[8] Hanswille G, Sedlacek G. Steel and Composite Bridges in Germany: State of the Art. Wuppertal: University of Wuppertal, Institute for Steel and Composite Structures; 2007.
[9] Kuhlmann, U., Braun, B., Feldmann, M. COMBRI Design Manual - Part II: State of-the-Art and Conceptual Design of Steel and Composite Bridges, Germany; 2008.
[10] He J, Liu Y, Chen A, Yoda T. Experimental study on inelastic mechanical behaviour of composite girders under hogging moment. J Constr Steel Res 2010;66(1):37–52.
[11] Lam D, El-Lobody E. Behaviour of headed stud shear connectors in composite beam. J Struct Eng 2005;131(1):96–107.
[12] Colajanni P, La Mendola L, Monaco A. Stress transfer mechanism investigation in hybrid steel trussed–concrete beams by push-out tests. J Constr Steel Res 2014;95:56–70.
[13] He J, Liu Y, Pei B. Experimental study of the steel-concrete connection in hybrid cable-stayed bridges. J Perform Constr Facil 2014;28(3):559–70.
[14] He J, Lin Z, Liu Y, Xu X, Xin H, Wang S. Shear stiffness of headed studs on structural behaviours of steel-concrete composite girders. Steel Comp Struct 2020;36(5):553–68.
[15] Lin W, Yoda T, Taniguchi N, Kasano H, He J. Mechanical performance of steel-concrete composite beams subjected to a hogging moment. J Struct Eng ASCE 2014;140(1):04013031.
[16] An L, Cederwall K. Push-out tests on studs in high strength and normal strength concrete. J Constr Steel Res 1996;36(1):15–29.
[17] Shim C, Lee P, Yoon T. Static behaviour of large stud shear connectors. Eng Struct 2004;26(12):1853–60.
[18] Lee P, Shim C, Chang P. Static and fatigue behaviour of large stud shear connectors for steel-concrete composite bridges. J Constr Steel Res 2005;61(9):1270–85.
[19] Pallarés L, Hajjar JF. Headed steel stud anchors in composite structures, Part I: Shear. J Constr Steel Res 2010;66(2):198–212.
[20] Xue D, Liu Y, Yu Z, He J. Static behaviour of multi-stud shear connectors for steel–concrete composite bridge. J Constr Steel Res 2012;74:1–7.
[21] Lin Z, Liu Y, He J. Behaviour of stud connectors under combined shear and tension loads. Eng Struct 2014;81:362–76.
[22] Dallam LN. Pushout tests with high strength bolt shear connectors. Rep. 68-7, Dept. of Civil Engineering, Univ. of MissouriColumbia, Columbia, MO; 1968.

[23] Dallam LN, Harpster JL. Composite beams tests with high-strength bolt shear connectors. Rep. 68-3, Dept. of Civil Engineering, Univ. of Missouri-Columbia, Columbia, MO. 1968.
[24] Marshall WT, Nelson HM, Banerjee HK. An experimental study of the use of high-strength friction-grip bolts as shear connectors in composite beams. Struct Eng 1971;49(4):171–8.
[25] Kwon G, Engelhardt MD, Klinger RE. Behavior of post-installed shear connectors under static and fatigue loading. J Constr Steel Res 2010;66:532–41.
[26] Kwon G, Engelhardt MD, Klingner RE. Experimental behavior of bridge beams retrofitted with post installed shear connectors. J Bridge Eng 2011;16(4):536–45.
[27] Pavlović, M. Resistance of Bolted Shear Connectors in Prefabricated Steel-Concrete Composite Decks, Ph.D. Thesis; University of Belgrade, Faculty of Civil Engineering, Belgrade, Serbia;. 2013.
[28] Pavlovic M, Markovic Z, Veljkovic M, Buđevac D. Bolted shear connectors vs. headed studs behaviour in push-out tests. J Constr Steel Res 2013;88:134–49.
[29] Liu X, Bradford M, Lee M. Behavior of high-strength friction-grip bolted shear connectors in sustainable composite beams. J Struct Eng ASCE 2015;141:04014149.
[30] Ataei A, Bradford MA, Liu X. Experimental study of composite beams having a precast geopolymer concrete slab and deconstructable bolted shear connectors. Eng Struct 2016;2016(114):1–13.
[31] Ataei A, Zeynalian M, Yazdi Y. Cyclic behaviour of bolted shear connectors in steel-concrete composite beams. Eng Struct 2019;198(1):109455.
[32] Yang F, Liu Y, Jiang Z, Xin H. Shear performance of a novel demountable steel-concrete bolted connector under static push-out tests. Eng Struct 2018;160:133–46.
[33] Lam D, Saveri E. Shear capacity of demountable shear connectors. Proceedings of the 10th International Conference on Advances in Steel Concrete Composite and Hybrid Structures. 2012.
[34] Moynihan MC, Allwood JM. Viability and performance of demountable composite connectors. J Constr Steel Res 2014;88:47–56.
[35] Dai X, Lam D, Saveri E. Effect of concrete strength and stud collar size to shear capacity of demountable shear connectors. J Struct Eng 2015;141(11):04015025.
[36] Rehman N, Lam D, Dai X, Ashour AF. Experimental study on demountable shear connectors in composite slabs with profiled decking. J Constr Steel Res 2016;122:178–89.
[37] Pathirana SW, Uy B, Mirza O, Zhu X. Strengthening of existing composite steel-concrete beams utilising bolted shear connectors and welded studs. J Constr Steel Res 2015;114:417–30.
[38] Pathirana SW, Uy B, Mirza O, Zhu X. Flexural behaviour of composite steel-concrete utilizing blind bolt shear connectors. Eng Struct 2016;114:181–94.
[39] Ban H, Uy B, Pathirana SW, Henderson I, Mirza O, Zhu X. Time-dependent behaviour of composite beams with blind bolts under sustained loads. J Constr Steel Res 2015;112:196–207.
[40] Henderson IEJ, Zhu XQ, Uy B, Mirza O. Dynamic behaviour of steel-concrete composite beams with different types of shear connectors. Part I: Experimental study. Eng Struct 2015;103:298–307.
[41] Henderson IEJ, Zhu XQ, Uy B, Mirza O. Dynamic behaviour of steel-concrete composite beams with different types of shear connectors. Part II: Modelling and comparison. Eng Struct 2015;103:308–17.
[42] Feidaki E, Vasdravellis G, He J, Wang S. Steel-yielding demountable shear connector for composite floors with precast hollow-core slab units. J Struct Eng 2019;145(8):04019076.
[43] He J, Vasdravellis G, Wang S. Circular perforated steel yielding demountable shear connector for sustainable precast composite floors. Steel Comp Struct 2021;39(6):701–21.
[44] Kozma A, Odenbreit C, Braun M, Veljkovic M, Nijgh M. Push-out tests on demountable shear connectors of steel-concrete composite structures. Structures 2019;21:45–54.
[45] Suwaed ASH, Karavasilis TL. Removable shear connector for steel-concrete composite bridges. Steel Comp Struct 2018;29(1):107–23.
[46] Suwaed ASH, Karavasilis TL. Demountable steel-concrete composite beam with full-interaction and low degree of shear connection. J Constr Steel Res 2020;171:106152.
[47] Suwaed ASH, Karavasilis TL. Novel demountable shear connector for accelerated disassembly, repair, or replacement of precast steel-concrete composite bridges. J Bridg Eng 2017;22(9):04017052.
[48] He J, Suwaed ASH, Vasdravellis G, Wang S. Shear performance of a novel demountable connector for reusable steel-concrete composite structures. Life-Cycle Civil Engineering: Innovation, Theory and Practice – Proceedings of the 7th International Symposium on Life-Cycle Civil Engineering, IALCCE 2020, 2020, pp. 775–781.
[49] Suwaed ASH, He J, Vasdravellis G. Experimental and numerical evaluation of a welded demountable shear connector through horizontal pushout tests. J Struct Eng 2022;148(2):04021274.
[50] He J, Suwaed ASH, Vasdravellis G. Horizontal pushout tests and parametric analyses of a locking-bolt demountable shear connector. Structures 2022;35:667–83.
[51] Eurocode 4. Design of composite steel and concrete structures. Part 1–1. General rules and rules for buildings. EN 1994-1-1. Brussels, Belgium: BSI; 2004.
[52] BSI (British Standards Institution). Testing hardened concrete, Part 3: Compressive strength of test specimens. BS EN 12390-6. London: BSI; 2009.
[53] ASTM. Standard test methods for tension testing of metallic materials. ASTM E8/E8M. West Conshohocken, PA: ASTM; 2011.
[54] ABAQUS (2018) [Computer software]. Providence, RI, Dassault Systemès Simulia.
[55] He J, Suwaed ASH, Vasdravellis G, Wang S. Standard pushout tests and design rules for a bolted-welded hybrid demountable shear connector. J Struct Eng 2022;148(8):04022097.
[56] *fib* (Fédération internationale du béton). 2010. First complete draft. Vol. 1. Comité Euro-International du Beton. In Model code 2010, secretariat permanent. Lausanne, Switzerland.
[57] Birtel, V., Mark, P. Parameterized finite element modelling of RC beam shear failure. The 19th Annual International ABAQUS Users' Conference, ABAQUS Inc, Boston, USA, 2006. pp. 95–108.
[58] Yang T, Liu S, Qin B, Liu Y. Experimental study on multi-bolt shear connectors of prefabricated steel-concrete composite beams. J Constr Steel Res 2020;173:106260.
[59] Rehman N. Behaviour of demountable shear connectors in composite structures. UK: University of Bradford; 2017. Ph. D dissertation.
[60] Pathirana SW, Uy B, Mirza O, Zhu X. Bolted and welded connectors for the rehabilitation of composite beams. J Constr Steel Res 2016;125:61–73.
[61] Zhang Y, Chen B, Liu A, Pi Y, Zhang J, Wang Y, et al. Experimental study on shear behavior of high strength bolt connection in prefabricated steel-concrete composite beam. Compos B Eng 2019;159:481–9.
[62] Suwaed ASH. Development of novel demountable shear connectors for precast steel-concrete composite bridges. Ph. D dissertation. UK: University of Warwick; 2017.
[63] American Institute of Steel Construction (AISC). Specification for Structural Steel Buildings. Standard No. ANSI/AISC 360–10. USA. 2010.
[64] American Concrete Institute (ACI). Building code Requirements for Structural Concrete. Standard No. ACI 318-08. USA. 2008.
[65] GB50017. Code for design of steel structures. Beijing; 2003.
[66] AASHTO. AASHTO LRFD bridge design specifications, Washington, DC; 2014.
[67] BSI (British Standards Institution). EN1993–1-8: Eurocode 3: Design of steel structures. Part 1–8: Design of joints, European Committee for standardization (CEN), Brussels Belgium; 2005.